

A general framework for validated continuation of periodic orbits in systems of polynomial ODEs

Jan Bouwe van den Berg* Elena Queirolo†

March 22, 2019

Abstract

In this paper a parametrized Newton-Kantorovich approach is applied to continuation of periodic orbits in arbitrary polynomial vector fields. This allows us to rigorously validate numerically computed branches of periodic solutions. We derive the estimates in full generality and present sample continuation proofs obtained using an implementation in Matlab. The presented approach is applicable to any polynomial vector field of any order and dimension. A variety of examples is presented to illustrate the efficacy of the method.

1 Introduction

A central question in dynamical systems is how the dynamics changes as a parameter is varied. These problems can be investigated numerically using powerful tools such as Auto [12], MatCont [11], PyDSTool [7], XPP [13] and COCO [9]. Indeed, the theory for numerical continuation and bifurcation analysis is well established, e.g. see [18]. One type of dynamics that is of particular interest are periodic motions, as they are often encountered in applications. In this paper we develop a general methodology to turn the numerical continuation computations of periodic orbits into *theorems*, i.e., we mathematically validate the numerical results by providing and proving explicit error estimates.

Our analysis builds on earlier work where such computer-assisted proof methods have been implemented in the context of specific example problems. For *initial* value problems rigorous integrators for general systems of ODEs exist, such as CAPD [4] and COSY [22]. Additionally, CAPD also has the capability to combine the rigorous integrator with well chosen Poincaré sections and topological tools to study periodic orbits. Another approach, which complements these phase space techniques, is to use a functional analytic setup to

*VU Amsterdam, Department of Mathematics, De Boelelaan 1081, 1081 HV Amsterdam, The Netherlands, janbouwe@few.vu.nl; partially supported by NWO-VICI grant 639033109.

†VU Amsterdam, Department of Mathematics, De Boelelaan 1081, 1081 HV Amsterdam, The Netherlands, e.queirolo@vu.nl

turn the search for periodic orbits into a zero finding problem. We refer to the work by Arioli and Koch (e.g. [1]), as well as the related “radii polynomial” technique, which has been applied to find periodic solutions in specific systems of ODEs arising in a variety of applications [27, 17, 21]. The functional analytic approach is particularly convenient for continuation problems. In the radii polynomial setting this was first introduced in [28, 3], and further explored in [15, 32, 19], see also [33] for a closely related perspective on computer-assisted continuation and bifurcation proofs. In the current paper we adopt the radii polynomial methodology within the functional analytic framework and develop it into a universal mathematically rigorous continuation tool for periodic orbits.

Whereas the efforts discussed above focus on specific equations, our main contribution is that we deal with the rigorous continuation of periodic orbits in *general* polynomial vector fields. In comparison to attacking example systems, setting up such a general approach requires a different gauging of the options at our disposal in order to derive comprehensive estimates which do not use any specific structure of the system. This somewhat more conceptual perspective, and the universal applicability of the theorems and code, are the main novelties of the current paper viewed against the backdrop of the existing literature.

To describe in more detail the results obtained in this paper, consider the problem

$$\begin{cases} \dot{u} = f(\mu, u) \\ g(\mu) = 0 \\ u(t) \text{ is periodic.} \end{cases} \quad (1)$$

The solution $u(t) \in \mathbb{R}^N$ is vector-valued, and $\mu \in \mathbb{R}^{M'}$ is a (set of) parameter(s). Throughout this paper and accompanying code the vector field $f : \mathbb{R}^{M'} \times \mathbb{R}^N \rightarrow \mathbb{R}^N$ is assumed to be polynomial (see below for a more nuanced statement about applicability to an even more general class of vector fields). The additional restrictions on the parameter(s) μ , described by $g : \mathbb{R}^{M'} \rightarrow \mathbb{R}^{M''}$, are again assumed to be of polynomial form. We note that determining the period L of the solution is part of the problem. Since the system is autonomous, solutions can be shifted in time. We lift this degeneracy by imposing a phase condition. The dimension count for the continuation problem then implies that for the case $M' - M'' = 1$ generically a solution of (1) is part of a one parameter family of periodic orbits. Such continuation problems can be tracked numerically, but non-rigorously, using a variety of powerful software packages [7, 9, 11, 12, 13]. In this paper we describe a computer-assisted procedure to justify *rigorously* the parametrized families of periodic solutions.

Hence, while we develop a general method, we do require the nonlinearities to be polynomial, both for practical and technical reasons. Indeed, the polynomial dependence of both f and g on the parameters μ is entirely for convenience. We need to have access to derivatives up to third order, and these are particularly easy to determine for polynomials. In particular, restricting to polynomials means that we do not need to consider automatic differentiation techniques in the implementation, nor do we require input of derivatives of f and g by the

user. But this is merely convenient: the estimates hold more generally for non-polynomial dependence on μ , see Section 2.5 for more details.

On the other hand, the assumption that the vector field f depends polynomially on u is of a somewhat more fundamental, although not essential, nature. The three main issues that arise are understood most easily when considering the Fourier transformed problem. Indeed, the first step in our technique is to formulate a zero finding problem, equivalent to (1), in a space of Fourier coefficients. The first advantage of looking at polynomial vector fields is that the solutions are real analytic, hence one may work in a space of geometrically decaying Fourier coefficients. The second technical advantage is that when some numerical approximation $\hat{u}(t)$ is described by finitely many nonzero Fourier coefficients (cf. Galerkin projection), then in the polynomial case the vector field $f(\mu, \hat{u}(t))$ again has finitely many nonzero Fourier coefficients, albeit more than $\hat{u}(t)$. The third advantage is that some of the estimates may be performed monomial by monomial (“term by term”).

By developing the computer-assisted rigorous framework in the context of general systems of *polynomial* ODEs, we strike a balance between generality and clarity. We do not regard this restriction as crucial for the method. When one wants to consider a non-polynomial vector field using the methods in this paper, there are two clear paths forward. One option is to introduce a change of variables which polynomializes the vector field, see e.g. [21, 26]. Another possibility is to use interpolation estimates as in [14] to control the extra terms appearing in the bounds. In the latter case, when the vector field is not analytic, one should change the weights in the norm to be algebraic rather than exponential, cf. [20]. We are confident that either approach can be readily combined with the methods presented in the current paper. Moreover, the framework for rigorously validated continuation in the radii polynomial setting can be extended to other types of solutions, such as heteroclinic orbits (see [31] for general single orbit validation of such solutions; a continuation result for a special case can be found in [25]).

Additional possible generalizations include replacing $g(\mu) = 0$ by equations of the form $g(\mu, u(0)) = 0$ and/or adding integral conditions. Furthermore, these methods can also be adapted to cases with symmetries (e.g. reversibility symmetry or Hamiltonian systems), e.g. see [27, 8], but such extensions are not explored in the current paper. Similarly, our approach is also applicable to delay-differential equations, see [26]. While we see no structural obstruction to such generalizations, in each case one will have to balance generality with complexity of the estimates and code. Finally, a natural counterpart of continuation is bifurcation analysis. In some instances bifurcation problems can in fact be attacked in a similar framework, see e.g. [1, 34, 19, 32], but many cases remain unexplored. In a forthcoming paper [29] we build on the current general continuation framework to analyze saddle-node bifurcations of branches of periodic orbits, as well as the branches emanating from equilibria at Hopf bifurcations.

Our method takes a numerical continuation technique as a starting point and builds a mathematical theorem on top of that. To outline the main steps,

we begin with numerical approximations of *two* solutions to (1), which one should imagine to be not too far apart. In Fourier space these are represented by Fourier coefficients \hat{u}^0 and \hat{u}^1 and parameter values $\hat{\mu}^0$ and $\hat{\mu}^1$, as well as approximate periods \hat{L}^0 and \hat{L}^1 . In practice only finitely many of the Fourier coefficients in both \hat{u}^0 and \hat{u}^1 are nonzero, since they result from a numerical computation on a truncated problem. The triples $[\hat{u}^s, \hat{\mu}^s, \hat{L}^s]$ for $s = 0, 1$ are both approximate zeros of a zero finding problem that is equivalent with (1). Using a Newton-like map, we turn that zero finding problem into an equivalent fixed point problem. We then show that near the line segment

$$\Sigma = \left\{ (1-s)[\hat{u}^0, \hat{\mu}^0, \hat{L}^0] + s[\hat{u}^1, \hat{\mu}^1, \hat{L}^1] : s \in [0, 1] \right\}$$

this fixed point problem has a curve of solutions. Although in this introduction we do not introduce the precise norms, the intuition is that we consider a cylinder around the line segment Σ with radius r , which we treat as a computational parameter. We then set out to prove that the fixed point operator is a contraction on this cylinder for each $s \in [0, 1]$, so that an application of the uniform Banach contraction theorem provides us with a (unique) curve of solutions within this cylinder. The crux is that we analytically derive conditions that guarantee this contraction property, and these conditions take the form of a *finite set of inequalities*, which turn out to be polynomial in the radius r , hence the name “radii polynomial” method.

As mentioned before, one of the main features of this paper is that the analytic bounds are applicable to arbitrary polynomials and do not require *ad hoc* computations to be applied to a new vector field, as long as it is polynomial. In particular, the order of the vector field and the dimension of the problem do not impact the algorithm for the computation of the bounds, although they do influence the computational cost.

The definition of the inequalities mentioned above involves the numerical approximations $[\hat{u}^s, \hat{\mu}^s, \hat{L}^s]$, $s = 0, 1$ as well as a numerically computed Jacobian of a truncated problem, and checking that the inequalities are satisfied for some r is not feasible by hand. This is where the computer-assisted part of the proof occurs: the finite set of inequalities is rigorously checked by computer using interval arithmetic. When the algorithm is successful, the combination of the general analytic estimates with the computer-assisted computations for a specific system generates a theorem saying that there is a one-parameter family of periodic orbits $[u(s), \mu(s), L(s)]$, $s \in [0, 1]$ of (1) within a cylinder with explicitly known radius r around the segment Σ (the precise definition of this cylinder is provided in (32)). Several of these segments can then be “glued” together to form a longer continuous curve of solutions. Since the radius r of the cylinder is determined explicitly, this gives direct error control on the distance between the solutions and the numerical segment Σ . The control in Fourier space also translates into explicit bounds in phase space, see Remark 4.3.

The outline of the paper is as follows. In Section 2 we introduce the representation in Fourier space of the ODE problem (1) and set up the necessary notation. In Section 3 we define the fixed point operator and the associated

radii polynomials. The symmetry considerations, which guarantee that the fixed points in Fourier space correspond to real-valued solutions of (1), are discussed in Section 4. In Section 5 some technical operator estimates are introduced, which are then applied in Section 6 to build the radii polynomial bounds for a single periodic solution to (1). These bounds are generalized to the continuation case in Section 8. Sections 6 and 8 thus together form the core of the paper. For clarity of exposition we elected to separate the issues related to single orbit validation (§6) from the effects of continuation, which are essentially appended in §8. In Section 7 we present some examples of single orbit validation, and we discuss the choices of computational parameters in this context. In Section 9 we explore some computational aspects of the continuation algorithm, including step size and mode number selection. Finally, to illustrate the general applicability of the results, in Section 10 we present examples of validated continuation.

As a final note, our implementation, which is available at [30], is in Matlab and uses Intlab [23] for the interval arithmetic part of the proofs. While we of course attempted to write efficient code, we did not put emphasis on optimizing computational time, but focused foremost on flexibility and transparency.

2 Reformulation in Fourier space

Since the period L of a solution to (1) is a priori unknown, we start by rescaling time, so that we can restrict attention to 2π periodic functions. We thus replace, without introducing new notation for the rescaled variables, $\dot{u} = f(\mu, u)$ by

$$\dot{u} = \tau f(\mu, u), \quad (2)$$

where $\tau = \frac{L}{2\pi}$ is the a priori unknown, normalized period.

Without worrying, for the moment, about convergence, we write the Fourier expansion of a 2π -periodic function $u = (u_1, \dots, u_N) : \mathbb{R} \rightarrow \mathbb{R}^N$ as

$$u(t) = \sum_{k \in \mathbb{Z}} (v)_k e^{ikt}, \quad (v)_k = (v_1, \dots, v_N)_k \in \mathbb{C}^N. \quad (3)$$

When needed, we will use the notation $(\mathcal{F}u_i)_k = (v_i)_k$ to indicate the k -th Fourier coefficient of the n -th component of the solution, while $(\mathcal{F}u)_k$ is a complex vector of length N containing the k -th Fourier coefficients of the vector valued function $u(t)$. In particular, in the notation we do not distinguish between the Fourier transform of a scalar-valued or vector-valued function; this should be clear from the context. Likewise, the inverse Fourier transform is denoted by $u_i(t) = \mathcal{F}^{-1}v_i$ and $u(t) = \mathcal{F}^{-1}v$.

The analogue of the system of ODEs (2) in Fourier space is

$$ik(v)_k = \tau(\mathcal{F}f(\mu, \mathcal{F}^{-1}v))_k. \quad (4)$$

We collect the parameters in $\lambda = (\tau, \mu_1, \dots, \mu_{M'})$ and introduce the notation

$$\hat{f}(\lambda, v) \stackrel{\text{def}}{=} \tau \mathcal{F}f(\mu, \mathcal{F}^{-1}v). \quad (5)$$

for the right hand side of (4), and \hat{f}_i , $i = 1, \dots, N$ are the components of \hat{f} .

The pointwise multiplication of two scalar valued functions corresponds, in Fourier space, to the convolution of their sequences of Fourier coefficient. To be concrete, the convolution product between two sequences v_1 and v_2 is defined as

$$(v_1 \cdot v_2)_k \stackrel{\text{def}}{=} \sum_{k' \in \mathbb{Z}} (v_1)_{k'} (v_2)_{k-k'}.$$

In fact, we have (assuming u_1 and u_2 are sufficiently smooth)

$$(\mathcal{F}(u_1 u_2)) = (\mathcal{F}(u_1) \cdot \mathcal{F}(u_2)),$$

and

$$v_1 \cdot v_2 = \mathcal{F}(\mathcal{F}^{-1}(v_1) \mathcal{F}^{-1}(v_2)).$$

To reduce the notational burden, throughout the remainder of the paper we will just denote this product by $v_1 v_2$ rather than $v_1 \cdot v_2$. This extends to arbitrary powers and products involving more than two sequences, and hence to polynomials. It will be useful to introduce the following convention for the zeroth power of $w \in \mathbb{C}^{\mathbb{Z}}$:

$$(w^0)_k = \delta_{k0}, \quad \text{for all } k \in \mathbb{Z}, \text{ with } \delta \text{ the Kronecker delta.}$$

With these conventions, \hat{f} as defined in (5) is polynomial in its input arguments, since f is. Indeed, they may be viewed as the same polynomial, just with a different interpretation of the product.

Remark 2.1. *The convolution of two sequences with a finite number of non-zero elements also has a finite number of non-zero elements. In particular, if v_i for $i = 1, \dots, m$ are Fourier sequences with the property that for every i there exists a K_i such that $(v_i)_k$ vanishes for $|k| > K_i$, then $(v_1 v_2 \cdots v_m)_k$ vanishes for $|k| > \sum_{i=1}^m K_i$.*

We collect all unknowns into the variable $x = (\lambda, v)$, where $\lambda \in \mathbb{C}^{M'+1}$ and $v = (v_1, \dots, v_N)$ and $v_n \in \mathbb{C}^{\mathbb{Z}}$ for $n = 1, \dots, N$. The problem (2) is equivalent to the infinite dimensional zero finding problem

$$F(x) = \{F_i(x)\}_{i=1}^N = 0,$$

where $F_i(x)$ is a bi-infinite sequence defined, for every $k \in \mathbb{Z}$, as

$$(F_i(x))_k \stackrel{\text{def}}{=} -ik(v_i)_k + (\hat{f}_i(\lambda, v))_k. \tag{6}$$

with \hat{f}_i , defined in (5), a convolution polynomial.

2.1 The Banach space

Since periodic solutions of polynomial vector fields are analytic, we will search for a solution in a space of exponentially decaying Fourier coefficients. For $\nu \geq 1$

(a computational parameter to be chosen in the algorithm), we introduce the ν -norm of a bi-infinite complex sequence $w \in \mathbb{C}^{\mathbb{Z}}$ as

$$\|w\|_{\nu} \stackrel{\text{def}}{=} \sum_{k \in \mathbb{Z}} |w_k| \nu^{|k|}. \quad (7)$$

It is well known that the space

$$\ell_{\nu}^1 \stackrel{\text{def}}{=} \{w \in \mathbb{C}^{\mathbb{Z}} : \|w\|_{\nu} < \infty\} \quad (8)$$

is a Banach space. In fact it is a Banach algebra with the convolution product

$$\|w\tilde{w}\|_{\nu} \leq \|w\|_{\nu} \|\tilde{w}\|_{\nu} \quad \text{for all } w, \tilde{w} \in \ell_{\nu}^1. \quad (9)$$

Remark 2.2. *If $\nu > 1$ and $w \in \ell_{\nu}^1$, then w represents the sequence of Fourier coefficients of a function that is analytic on a strip of width $2 \log \nu$ around the real axis in the complex plane.*

Since the collection of unknowns is $x = (\lambda, v)$, where $\lambda = (\tau, \mu_1, \dots, \mu_{M'})$ are the $M' + 1$ scalar parameters and v represents N Fourier sequences, we introduce the product space $X = X_{\nu} := \mathbb{C}^M \times (\ell_{\nu}^1)^N$, where $M = M' + 1$. We endow X with the norm

$$\|x\|_X = \|(\lambda, v)\|_X = \max\{|\lambda_1|, \dots, |\lambda_M|, \|v_1\|_{\nu}, \dots, \|v_N\|_{\nu}\}. \quad (10)$$

We will also use the notation x_n to indicate the n -th component of x :

$$x_n = \begin{cases} \lambda_n & \text{if } 1 \leq n \leq M, \\ v_{n-M} & \text{if } M + 1 \leq n \leq M + N, \end{cases}$$

and the componentwise norm

$$\|x_n\| = \begin{cases} |x_n| & \text{if } 1 \leq n \leq M, \\ \|x_n\|_{\nu} & \text{if } M + 1 \leq n \leq M + N. \end{cases} \quad (11)$$

Remark 2.3. *It is a straightforward and natural generalization to incorporate weights in the norm (10) on X . Since this is equivalent to rescaling the components of the parameter vector μ (and hence λ) and/or the vector field u (and hence v), all estimates in this paper have natural analogues for such a weighted norm. In order not to overburden the notation, we did not pursue such weighted norms in the current paper. We refer to [32] for an extensive discussion of an application where weighted norms are essential.*

2.2 Finite dimensional projections

In order to carry out numerical computations, which underlie our validated continuation results, we need to truncate the infinite dimensional problem. In particular, to construct numerical approximations of the solutions, we consider a finite dimensional Galerkin projection of X based on $2K + 1$ Fourier coefficients, with $K \in \mathbb{N}$ a computational parameter.

Definition 2.4. For $K \in \mathbb{N}$, we define $\tilde{\Pi}_K$ as the projection that maps ℓ_ν^1 into \mathbb{C}^{2K+1} via

$$\tilde{\Pi}_K w \stackrel{\text{def}}{=} (w_{-K}, w_{-K+1}, \dots, w_0, \dots, w_{K-1}, w_K) \in \mathbb{C}^{2K+1}.$$

The range of $\tilde{\Pi}_K$ can be naturally identified with a $2K+1$ dimensional subspace of ℓ_ν^1 by zero-padding. This natural embedding of \mathbb{C}^{2K+1} into ℓ_ν^1 will be denoted by $\tilde{\mathbf{E}}$. We will write $\tilde{\mathbf{\Pi}}_K \stackrel{\text{def}}{=} \tilde{\mathbf{E}}\tilde{\Pi}_K$.

We extend these operators to $x = (\lambda, v) \in X$ as follows:

$$\Pi_K x \stackrel{\text{def}}{=} (\lambda_1, \dots, \lambda_M, \tilde{\Pi}_K v_1, \dots, \tilde{\Pi}_K v_N) \in \mathbb{C}^M \times (\mathbb{C}^N)^{(2K+1)}.$$

The range of Π_K can be naturally identified with a $M + N(2K+1)$ dimensional subspace of X by applying $\tilde{\mathbf{E}}$ to the v components of $\Pi_K x$. The natural embedding of $\mathbb{C}^{M+N(2K+1)}$ into X will be denoted by \mathbf{E} . We will write $\mathbf{\Pi}_K \stackrel{\text{def}}{=} \mathbf{E}\Pi_K$.

We also introduce notation for the complementary, infinite tail of x :

$$\mathbf{\Pi}_K^\infty x \stackrel{\text{def}}{=} x - \mathbf{\Pi}_K x. \quad (12)$$

Furthermore, when $x = \mathbf{\Pi}_K x$, then we say that x has (at most) K non-zero modes.

When convenient, we will denote elements of $\Pi_K X$ by $\hat{x} = (\hat{\lambda}, \hat{v})$. In particular, numerical approximations of solutions will always be described by finitely many Fourier modes. Indeed, they are of the form $\mathbf{E}\hat{x} \in \mathbf{\Pi}_K X$, where $\hat{x} \in \mathbb{C}^{M+N(2K+1)}$ is stored in the computer. As we will see in Section 2.3, it is convenient to introduce the bilinear form

$$\langle \hat{x}, \hat{x}' \rangle \stackrel{\text{def}}{=} \sum_{j=1}^M \hat{\lambda}_j \hat{\lambda}'_j + \sum_{i=1}^N \sum_{k=-K}^K (\hat{v}_i)_k (\hat{v}'_i)_k \quad \text{on } \Pi_K X. \quad (13)$$

2.3 Phase condition and continuation equation

In terms of the collection of variables $x = (\lambda, v) = ((\tau, \mu), v)$ the equations we want to solve are $F(x) = 0$ and $g(\mu) = 0$. Whenever convenient we will write $g(x)$ for $g(\mu)$. This problem suffers from translation invariance, hence we introduce a phase condition $G^\mathbb{C}(x) = 0$ below, see (18). As explained in the introduction, for $M' = M'' + 1$ periodic orbits of (1), or equivalently, solutions of the system

$$\begin{cases} F(x) = 0, \\ g(x) = 0, \\ G^\mathbb{C}(x) = 0, \end{cases} \quad (14)$$

generically come in one-parameter families. To parametrize such a family and bring it into a form where we can use a contraction argument (and thus local uniqueness), we will additionally introduce a *continuation equation*, see (19).

To set the scene, let us assume to have two approximate solutions $\mathbf{E}\hat{x}_0$ and $\mathbf{E}\hat{x}_1$ of the system (14), although (for technical reasons) the equation for phase condition may be different for each: $G_s^{\mathbb{C}}(\mathbf{E}\hat{x}_s) = 0$ for $s = 0, 1$. If the distance between \hat{x}_0 and \hat{x}_1 is small, we can hope that the segment connecting these two points approximates a continuous branch of solutions. With this goal in mind, we define

$$x_s \stackrel{\text{def}}{=} \mathbf{E}[(1-s)\hat{x}_0 + s\hat{x}_1], \quad \text{for all } s \in [0, 1]. \quad (15)$$

Our goal is to “validate” this segment in the sense that we prove the existence of a unique curve of solutions to (1) in a cylinder of calculated radius centered around this segment. We now first introduce the (parametrized) phase conditions, and subsequently the continuation equation.

To quotient out the translation invariance of solutions, we choose a convenient phase condition which is linear and depends on finitely many Fourier modes only:

$$\sum_{i=1}^N \sum_{k=-K}^K (v_i)_k (q_i)_k - \tilde{q} = 0, \quad (16)$$

for some choices $\tilde{q} \in \mathbb{C}$, $q_i \in \mathbb{C}^{2K+1}$.

Remark 2.5. *In the choice of our standard phase condition we follow [6]. We choose a reference orbit, which in our case will be the numerical approximation \hat{u} , and require*

$$\int_0^{2\pi} \sum_{i=1}^N u_i(t) \hat{u}'_i(t) dt = 0.$$

In terms of Fourier coefficients this corresponds to the choice

$$(q_i)_k = ik(\hat{x}_i)_{-k}, \quad (17)$$

where \hat{x} are the (finitely many) Fourier coefficients of \hat{u} , and $\tilde{q} = 0$.

In the continuation problem it is convenient to vary the phase condition, hence we choose q^0 and q^1 associated to \hat{x}_0 and \hat{x}_1 . The idea is that the distance between q^0 and q^1 is small whenever the distance between \hat{x}_0 and \hat{x}_1 is small, see also Remark 2.5

We then formulate the phase condition using the bilinear form (13). We extend q^0 and q^1 , which both represent $N(2K+1)$ Fourier modes, see (17), to elements $\hat{q}_s = (0, q^s) \in \Pi_K X$, $s = 0, 1$, so that we can apply the bilinear form notation (13). Indeed, we write an interpolated version of (16) as $G_s^{\mathbb{C}}(x) = 0$, where

$$G_s^{\mathbb{C}}(x) \stackrel{\text{def}}{=} \langle \Pi_K x, \hat{q}_s \rangle - [(1-s)\langle \hat{x}_0, \hat{q}_0 \rangle + s\langle \hat{x}_1, \hat{q}_1 \rangle], \quad (18)$$

with

$$\hat{q}_s \stackrel{\text{def}}{=} (1-s)\hat{q}_0 + s\hat{q}_1, \quad \text{for all } s \in [0, 1].$$

We denote by $\tilde{H}_s(x) = (G_s^{\mathbb{C}}(x), g(x), F(x))$ the set of equations approximately satisfied by $\mathbf{E}\hat{x}_s$ for $s = 0, 1$. In order to parametrize a solution curve

close to the segment $\{x_s : s \in [0, 1]\}$ given by (15), we introduce a “fibration” of a cylindrically shaped neighborhood around this segment. We assume we have computed nontrivial vectors $\mathbf{E}\tilde{x}_0$ and $\mathbf{E}\tilde{x}_1$ that lie approximately in the null spaces of $D\tilde{H}_0(\mathbf{E}\hat{x}_0)$ and $D\tilde{H}_1(\mathbf{E}\hat{x}_1)$, respectively. We note that these null spaces are expected to be one dimensional since $M' = M'' + 1$. Moreover, we expect that \tilde{x}_0 and \tilde{x}_1 are close when \hat{x}_0 and \hat{x}_1 are close. Indeed, they are both approximately tangent to the solution curve, hence by choosing their lengths and orientations appropriately, in practice the “predictors” \tilde{x}_0 and \tilde{x}_1 are close together when the step size is not too large.

In view of the relation between the bilinear form (13) and the complex inner product on $\Pi_K \mathcal{S}$ we define

$$\hat{x}_s \stackrel{\text{def}}{=} \overline{\tilde{x}_s} \quad \text{for } s = 0, 1,$$

where the complex conjugate is taken elementwise in $\mathbb{C}^{M+(2K+1)N}$. We then introduce the continuation equation

$$G_s^\odot(x) \stackrel{\text{def}}{=} \langle \Pi_K x, \hat{x}_s \rangle - [(1-s)\langle \hat{x}_0, \hat{x}_0 \rangle + s\langle \hat{x}_1, \hat{x}_1 \rangle] = 0, \quad (19)$$

where

$$\hat{x}_s \stackrel{\text{def}}{=} (1-s)\hat{x}_0 + s\hat{x}_1, \quad \text{for all } s \in [0, 1].$$

Interpolating between \hat{x}_0 and \hat{x}_1 in this way is convenient when we glue together multiple solution segments, see Remark 3.5 and [3]. We remark that the expressions for G_s^\odot and G_s^\odot are affine *linear* in both x and s , which is a useful simplification in comparison with the approach in [3].

2.4 The zero finding problem

We collect the continuation equation, the phase condition, and the scalar conditions in

$$G_s(x) = \begin{pmatrix} G_s^\odot(x) \\ G_s^\odot(x) \\ g(x) \end{pmatrix}, \quad (20)$$

which maps X to \mathbb{C}^M , where $M = M' + 1 = M'' + 2$. Writing $x = (\lambda, v) = ((\tau, \mu), v)$, we note that G_s^\odot depends on v only, whereas g depends only on μ , but G_s^\odot depends on all variables in $\Pi_K X$. For every $s \in [0, 1]$ the full zero finding problem for continuation of periodic orbits becomes

$$H_s(x) \stackrel{\text{def}}{=} \begin{pmatrix} G_s(x) \\ F(x) \end{pmatrix} = 0. \quad (21)$$

We note that H_s does not map X_ν into itself, but it does map X_ν to $X_{\nu'}$ for any $\nu' < \nu$. This slight subtlety is of no consequence and will henceforth not be addressed explicitly.

We will also number the equations in (21) as $H = (H_{[1]}, \dots, H_{[M+N]})$. This cumbersome notation is to distinguish H_1 , which represents H_s when $s = 1$,

from the first component $H_{[1]} = G_s^\odot$ of H . In particular, by H_1 we mean the continuation equation, never H_s for $s = 1$. When, as in Sections 6 and 7, we ignore continuation, either by fixing s or by setting $\hat{x}_0 = \hat{x}_1$, $\hat{q}_0 = \hat{q}_1$, and $\hat{x}_0 = \hat{x}_1$, then we denote the resulting s -independent set of equations by $H(x) = (G(x), F(x)) = 0$.

The truncated problems \hat{H}_s for $s = 0, 1$, which is used for numerical computations, is defined by

$$\begin{aligned} \hat{H}_s : \mathbb{C}^M \times (\mathbb{C}^N)^{(2K+1)} &\mapsto \mathbb{C}^M \times (\mathbb{C}^N)^{(2K+1)} \\ \hat{H}_s(\hat{x}) &= \Pi_K H_s(\mathbf{E}\hat{x}) \quad \mathbf{s} = 0, 1. \end{aligned} \quad (22)$$

The finite dimensional problem $\hat{H}_s(\hat{x}) = 0$ can be solved numerically when one has a reasonable guess for a solution, for example using Newton's method.

2.5 Interval arithmetic and notation for derivatives

A crucial step in our computer-assisted proofs is to check finitely many inequalities, see (35). To accomplish this we use interval arithmetic, in particular the Intlab [23] package for Matlab. While the details (and implementation) of interval arithmetic are beyond the scope of the current paper, we will frequently evaluate polynomials *in an interval arithmetic sense* as explained below. We will assume we have access to all partial derivatives up to order 3 of the rescaled nonlinearity

$$\tilde{f}(\lambda, u) = \tilde{f}(\lambda, u) \stackrel{\text{def}}{=} \tau f(\mu, u)$$

as well as the scalar equations represented by $\tilde{g}(\lambda) = \tilde{g}(\tau, \mu) \stackrel{\text{def}}{=} g(\mu)$, namely

$$D^\alpha \tilde{f}_i \quad \text{and} \quad D^\alpha \tilde{g}_j$$

for multi-indices $\alpha = (\alpha_1, \dots, \alpha_{N+M})$ with

$$|\alpha| \stackrel{\text{def}}{=} \sum_{n=1}^{N+M} \alpha_n \leq 3.$$

In particular, we can evaluate all of these in interval sense, i.e., we have computable bounds

$$D^\alpha \tilde{f}_i(I_1, \dots, I_{M+N}) \supset \{D^\alpha \tilde{f}_j(y_1, \dots, y_{M+N}) : y_n \in I_n\}$$

for any intervals $I_n \subset \mathbb{R}$, and similarly for \tilde{g} .

As already explained in the introduction, our implementation is for polynomial \tilde{f} and \tilde{g} . All estimates in the paper hold as long as the dependence of \tilde{f} on u is polynomial. The dependence of \tilde{f} and \tilde{g} on λ may be non-polynomial as long as we can evaluate them, and their derivatives up to third order, in an interval arithmetic sense. In this paper, to reduce some of the technicalities, we work in the complex setting, hence we assume $\tilde{g}(\mu)$ to be real analytic (on the relevant domain of parameter values), and similarly for the dependence on μ of

the coefficients in the polynomial vector field \tilde{f} , see (23). We note that working in the fully complex setting, while convenient, is not necessary, and the method can be extended to C^3 dependence on μ , cf. [26].

Concerning the polynomial dependence of \tilde{f} on u , it will be useful to introduce notation to express \tilde{f} and its derivatives in terms of monomials. We can write for any $\alpha \in \mathbb{N}^{N+M}$ and $i = 1, \dots, N$

$$D^\alpha \tilde{f}_i(\lambda, u) = \sum_{\beta \in \mathcal{D}(\alpha, i)} \tilde{f}_{\beta, \alpha, i}(\lambda) \prod_{i'=1}^N u_{i'}^{\beta_{i'}} \quad (23)$$

for some *finite* set $\mathcal{D}(\alpha, i) \subset \mathbb{N}^N$ of multi-indices. We assume that we can evaluate these coefficient functions $\tilde{f}_{\beta, \alpha, i} : \mathbb{R}^M \rightarrow \mathbb{R}$ for any $|\alpha| \leq 3$, $i = 1, \dots, N$ and $\beta \in \mathcal{D}(\alpha, i)$, and similarly for their derivatives (with respect to λ) up to order $3 - |\alpha|$.

In Fourier space, the derivatives of $\hat{f}(\lambda, v)$ with respect to v can be naturally expressed as Toeplitz operators. Indeed, for any $w \in \ell_\nu^1$ we define the Toeplitz operator $\mathcal{T}_w \in B(\ell_\nu^1)$ by $\mathcal{T}_w \tilde{w} \stackrel{\text{def}}{=} w \cdot \tilde{w}$, which we express elementwise as

$$(\mathcal{T}_w \tilde{w})_k = \sum_{k' \in \mathbb{Z}} (\mathcal{T}_w)_{kk'} \tilde{w}_{k'} \quad \text{where } (\mathcal{T}_w)_{kk'} = w_{k-k'}. \quad (24)$$

The expressions for the derivatives can be lifted to Fourier space by interpreting the product in the convolution sense. We denote the convolution polynomial corresponding to $D^\alpha \hat{f}_j(\lambda, v)$ by

$$\hat{f}_i^\alpha(\lambda, v) = \sum_{\beta \in \mathcal{D}(\alpha, i)} \tilde{f}_{\beta, \alpha, i}(\lambda) \prod_{i'=1}^N v_{i'}^{\beta_{i'}}.$$

With this notation we can express the first derivatives, for any $i, i' = 1, \dots, N$, as

$$\partial_{v_i} \hat{f}_j(\lambda, v) = \mathcal{T}_{\hat{f}_j^{e_{M+i}}(\lambda, v)},$$

with unit multi-index vector $(e_n)_{n'} = \delta_{nn'}$.

To structure the components of the derivative of $H(\lambda, v) = (G(\lambda, v), F(\lambda, v))$ it is useful to use the natural decomposition of a (possibly unbounded) linear operator B on the product space $X = \mathbb{C}^M \times (\ell_\nu^1)^N$. Let $x = (\lambda, v)$, then we write

$$(Bx)_n = \sum_{m=1}^M B_{nm} \lambda_m + \sum_{m=M+1}^{M+N} B_{nm} v_{m-M}, \quad \text{for } n = 1, \dots, M+N, \quad (25)$$

with linear operators $B_{nm} : X_m \rightarrow X_n$, where

$$X_n \stackrel{\text{def}}{=} \begin{cases} \mathbb{C} & \text{for } 1 \leq n \leq M \\ \ell_\nu^1 & \text{for } M+1 \leq n \leq M+N. \end{cases} \quad (26)$$

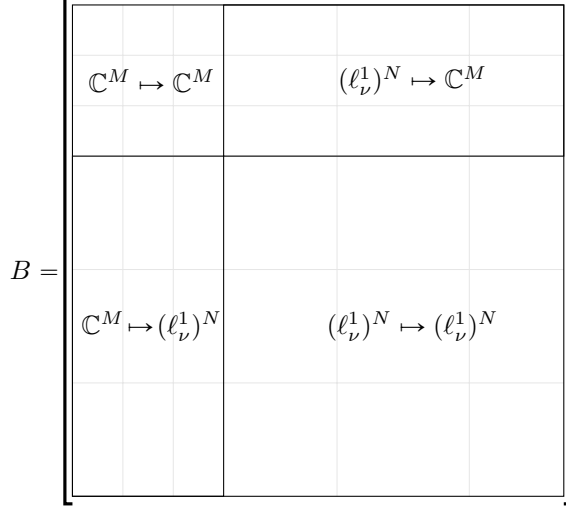


Figure 1: Representation of the matrix introduced in Equation (25).

To describe more explicitly the different components of B we observe that $B_{nm} \in \mathbb{C}$ for $m, n = 1, \dots, M$. For $n = 1, \dots, M$ and $m = M + 1, \dots, M + N$ the operator B_{nm} can be identified with a bi-infinite row vector, often an element of the dual of ℓ_ν^1 . For $n = M + 1, \dots, M + N$ and $m = 1, \dots, M$ analogously B_{nm} is a bi-infinite column vector, often an element of ℓ_ν^1 . Finally, for $m, n = M + 1, \dots, M + N$ the operator B_{nm} is described naturally by a bi-infinite matrix. The decomposition is represented graphically in Figure 1.

The components of the linear operator $D_m H_{[n]}$ thus split into derivatives $D_m G_n$ for $n = 1, \dots, N$ and derivatives $D_m F_{n-M}$ for $n = M + 1, \dots, M + N$. For the former case there is a further natural splitting into $n = 1, 2$, the continuation equation and phase condition, and $n = 3, \dots, M$, the algebraic constraints. In particular, for $n = 1$ we have

$$D_m H_{[1]}(x) = D_m G_s^\odot(x) = \begin{cases} (\dot{\lambda}_s)_m & \text{for } m = 1, \dots, M, \\ (\dot{v}_s)_{m-M}^T & \text{for } m = M + 1, \dots, M + N, \end{cases}$$

where $\dot{x}_s = (\dot{\lambda}_s, \dot{v}_s)$, and the transpose indicates the interpretation as an element of the dual of ℓ_ν^1 . For $n = 2$ we obtain

$$D_m H_{[2]}(x) = D_m G_s^\zeta(x) = \begin{cases} 0 & \text{for } m = 1, \dots, M, \\ (\hat{q}_s^v)_{n-M}^T & \text{for } m = M + 1, \dots, M + N, \end{cases}$$

where \hat{q}_s^v is the v -component of \hat{q}_s introduced in Section 2.3. For $n = 3, \dots, M$ the derivative is

$$D_m H_{[n]}(x) = D_m G_n(x) = \begin{cases} D^{e_m} \tilde{g}_{n-2}(\lambda) & \text{for } m = 1, \dots, M, \\ 0 & \text{for } m = M + 1, \dots, M + N. \end{cases}$$

Finally, for $n = M + 1, \dots, M + N$ we have

$$D_m H_{[n]}(x) = D_m F_{n-M}(x) = \begin{cases} \widehat{f}_{n-M}^{e_m}(x) & \text{for } m = 1, \dots, M. \\ \delta_{mn} \mathbf{k} + \mathcal{T}_{\widehat{f}_{n-M}^{e_m}(x)} & \text{for } m = M + 1, \dots, M + N. \end{cases} \quad (27)$$

with the (unbounded) diagonal operator \mathbf{k} defined by (with $w \in \mathbb{C}^{\mathbb{Z}}$)

$$(\mathbf{k}w)_k = kw_k \quad \text{for } k \in \mathbb{Z}. \quad (28)$$

Remark 2.6. *Instead of the description of the derivatives $\partial_{v_{i'}} \widehat{f}_i$ in terms of Toeplitz operators, one may equivalently write*

$$\partial_{v_{i'}} \widehat{f}_i(\lambda, v)w = \widehat{f}_i^{e_{M+i'}}(\lambda, v)w,$$

interpreting the right-hand side as a convolution multiplication. In this way we can identify $\partial_{v_{i'}} \widehat{f}_i(\lambda, v)$ with $\widehat{f}_i^{e_{M+i'}}(\lambda, v)$. This type of identification generalizes easily to higher derivatives of \widehat{f} (whereas the Toeplitz operator representation does not), for example

$$\begin{aligned} \partial_{v_{i''}} \partial_{v_{i'}} \widehat{f}_i(\lambda, v) &= \widehat{f}_i^{e_{M+i'} + e_{M+i''}}(\lambda, v), \\ \partial_{\lambda_j} \partial_{v_{i'}} \widehat{f}_i(\lambda, v) &= \widehat{f}_i^{e_j + e_{M+i'}}(\lambda, v). \end{aligned}$$

3 The radii polynomials

In this section we discuss how to turn the zero finding problem into a fixed point problem in such a way that we can check contractivity of the fixed point operator with the assistance of a computer. To construct the fixed point operator we apply a quasi-Newton approach. In particular, we define

$$T_s(x) \stackrel{\text{def}}{=} x - A_s H_s(x), \quad T_s : X \mapsto X, \quad s \in [0, 1]. \quad (29)$$

Here A_s is an injective map that approximates the inverse of the derivative of H_s in x_s . While we postpone the details of the construction of A_s to Section 8, we outline the construction here in order to give proper context for the central theorem below. We want A_s to be at the same time a good approximation of the inverse of $DH_s(\hat{x}_s)$ and simple enough to handle from a numerical and analytical point of view. With this in mind, we choose A_s as a linear interpolation in s of the approximate inverses of the derivatives $DH_0(\mathbf{E}\hat{x}_0)$ and $DH_1(\mathbf{E}\hat{x}_1)$, i.e., $A_s = (1 - s)A_0 + sA_1$ with

$$A_0 \approx (DH_0(\mathbf{E}\hat{x}_0))^{-1} \quad \text{and} \quad A_1 \approx (DH_1(\mathbf{E}\hat{x}_1))^{-1}.$$

The precise way in which A_s is an approximate inverse of $DH_s(\hat{x}_s)$ is encoded in the estimate (31). The required simplicity is achieved by imposing a block structure on A_0 and A_1 , in particular splitting the operators into a “finite part” and an “infinite diagonal tail”, as made explicit in Section 6.1.

Since for injective A_s (checking this injectivity is part of the proof in our setup, see Section 8.5) zeros of H_s and fixed points of T_s are in one-to-one correspondence, we set out to prove that this operator is a contraction map around the numerical segment $\{x_s : s \in [0, 1]\}$. In order to prove the contraction, we need two types of bounds, which we will call Y and $Z(r)$ bounds, indicating, respectively, the residual error of the approximate fixed point x_s defined in (15), and a bound on the derivative of T_s in a ball of radius r around this approximate fixed point.

Recalling that $x_s \in \mathbb{C}^M \times (\ell_\nu^1)^N$ consists of M scalars and N bi-infinite vectors, we introduce bounds $Y = (Y_1, \dots, Y_{N+M})$ and $Z(r) = (Z_1, \dots, Z_{M+N})(r)$ which are required to satisfy

$$Y_n \geq \max_{s \in [0, 1]} \|(T_s(x_s) - x_s)_n\|, \quad \text{for } n = 1, \dots, M + N, \quad (30)$$

and

$$Z_n(r) \geq \max_{s \in [0, 1]} \sup_{b, c \in B_1(0)} \|[DT_s(x_s + rb)rc]_n\|, \quad \text{for } n = 1, \dots, M + N, \quad (31)$$

with the notation for the norm introduced in (11) and with $B_1(0) \subset X$ the ball of radius 1 centered at the origin.

To prove contraction of the map T_s in the ball $B_r(x_s)$ for every s , it is now sufficient to find an r such that $Y_n + Z_n(r) < r$ for every n , as stated in the following theorem. We define the ‘‘cylinder’’

$$\mathcal{C}_r \stackrel{\text{def}}{=} \bigcup_{s \in [0, 1]} B_r(x_s) \quad (32)$$

of radius r around the segment $\{x_s : s \in [0, 1]\}$ of numerical approximations. We note that \mathcal{C}_r is in fact a pill-shaped neighborhood of the line segment.

Theorem 3.1. *Assume Y and $Z(r)$ satisfy in (30) and (31). We define*

$$p_n(r) \stackrel{\text{def}}{=} Y_n + Z_n(r) - r, \quad \text{for } n = 1, \dots, M + N. \quad (33)$$

If there exists an \hat{r} such that $p_n(\hat{r}) < 0$ for all $n = 1, \dots, M + N$, then T_s is a contraction on $B_{\hat{r}}(x_s)$ for every s in $[0, 1]$.

Assume moreover that A_s is injective for all $s \in [0, 1]$. Then the fixed points $x_{\text{sol}}(s)$ of T_s in $B_{\hat{r}}(x_s)$ form a continuous parametrized curve $x_{\text{sol}} : [0, 1] \rightarrow X$ in $\mathcal{C}_{\hat{r}}$, such that $H_s(x_{\text{sol}}(s)) = 0$ for every $s \in [0, 1]$.

Proof. For the proof we refer to [17], where in Proposition 1 this statement is proven for any fixed $s \in [0, 1]$. It is straightforward to infer that by using the uniform contraction mapping theorem that the fixed points form a continuous curve, see e.g. [28, 3] for more details. \square

Remark 3.2. *At this point there is still some work to do to show that the zeros of H_s that we have found correspond to real-valued orbits of the vector field (1). We will come back to this in Section 4. There we also list the explicit error bounds on the solution (i.e. the distance to the numerical approximation), see Remark 4.3.*

In order to guarantee smoothness of the solution curve, we use the following lemma.

Lemma 3.3. *With the hypotheses as in Theorem 3.1, assume in addition that for any $s \in [0, 1]$ and any $b \in B_1(0)$ we have*

$$\hat{r} \langle b, \dot{\hat{x}}_1 - \dot{\hat{x}}_0 \rangle \neq \langle \hat{x}_1 - \hat{x}_0, (1-s)\dot{\hat{x}}_1 + s\dot{\hat{x}}_0 \rangle. \quad (34)$$

Then $x_{\text{sol}} : [0, 1] \rightarrow X$ represents a smooth curve.

Proof. When $\partial_s E_s^\odot \neq 0$, the implicit function theorem provides the asserted smoothness, see [28, 3] for more details. Let $x \in \mathcal{C}_r$, then we can write $x = x_s + b$ for some $s \in [0, 1]$ and $b \in B_1(0)$. A direct computation shows that

$$\partial_s E_s^\odot(x) = r \langle b, \dot{\hat{x}}_1 - \dot{\hat{x}}_0 \rangle - \langle \hat{x}_1 - \hat{x}_0, (1-s)\dot{\hat{x}}_1 + s\dot{\hat{x}}_0 \rangle. \quad \square$$

Remark 3.4. *Since in practice \hat{x}_0 and \hat{x}_1 are close to each other, and $\hat{x}_1 - \hat{x}_0$ lies roughly in the direction of these predictors, the inequality (34) is expected to hold for sufficiently small \hat{r} . The righthand side of (34) can be bounded uniformly for $s \in [0, 1]$ using an interval arithmetic calculation. Moreover, since the bilinear form (13) involves a finite sum only, we can bound the lefthand side of (34) by enclosing it uniformly for $b \in \Pi_K B_1(0)$ using interval arithmetic.*

Remark 3.5. *The interpolations chosen in the definitions of $G_s^\mathbb{C}$ and G_s^\odot make it easy to “glue” subsequent steps of the continuation together to form a continuous (even smooth) curve. Indeed, following the arguments used in [3, 32], we conclude that if we choose the data \hat{x}_s , \hat{x}_s and \hat{q}_s in the end point of the previous step identical to those in the starting point of the next step, then the two parametrized curves of solutions obtained from Theorem 3.1 connect smoothly.*

The formulas introduced in (33) are often called radii polynomials [10], as the dependence of Z on r is usually polynomial. These radii polynomials capture the central idea that the continuation problem for solutions of (1) can be reduced to checking finitely many inequalities

$$p_n(\hat{r}) < 0 \quad \text{for } n = 1, \dots, M + N. \quad (35)$$

We denote by $\mathbf{I} = (r_{\min}, r_{\max})$ an interval on which we can prove that all radii polynomials are negative. We will call \mathbf{I} the interval of validation. Theorem 3.1 states that any r in \mathbf{I} is the radius of a cylinder \mathcal{C}_r , see (15), in which the existence and uniqueness of a branch of solutions is guaranteed.

4 Symmetry considerations

Since we are looking for real-valued periodic solutions of the ODE (1), its Fourier coefficients are conjugate symmetric in the following sense. For $w \in \ell_\nu^1$ we define the conjugate w^* as $w_k^* = \overline{w_{-k}}$. An element $w \in \ell_\nu^1$ is conjugate symmetric if $w = w^*$. We denote the space of conjugate symmetric sequences by $\ell_\nu^{\text{sym}} =$

$\{w \in \ell_\nu^1 : w = w^*\}$. With this definition, periodic orbits have Fourier coefficients $u_n \in \ell_\nu^{\text{sym}}$ for all $n = 1, \dots, N$ and some $\nu > 1$.

We generalize this notation of conjugation to X by setting

$$x^* = (\lambda, v)^* = (\overline{\lambda_1}, \dots, \overline{\lambda_M}, v_1^*, \dots, v_N^*).$$

We introduce the space of (conjugate) symmetric elements $\mathcal{S} \subset X = \mathbb{C}^M \times (\ell_\nu^1)^N$:

$$\mathcal{S} = \mathcal{S}_\nu \stackrel{\text{def}}{=} \{x \in X : x^* = x\}. \quad (36)$$

We look for a solution in this space of (conjugate) symmetric elements, and we will also choose our numerical approximation in \mathcal{S} . Nevertheless, we use the full space to perform our validation proof because of the ease of performing analysis on unrestricted double sided convolutions. In particular, we do not restrict to symmetric cases where sine or cosine series can be used. Such cases have been studied extensively, see e.g. [27, 3, 2, 17, 21]. Furthermore, we do not split into real and imaginary parts (cf. [19]) but rather recover conjugate symmetry a posteriori using the symmetry properties discussed below.

We now derive the results needed to prove that the fixed point of T_s found in Theorem 3.1 lies in \mathcal{S} , provided we choose a symmetry preserving linear operator A_s in the definition (29) of T_s . First we note that ℓ_ν^{sym} is closed under convolution multiplication. Moreover, for any $x = (\lambda, v) \in \mathcal{S}$ any polynomial expression in v with real coefficients (depending on $\lambda \in \mathbb{R}^M$) also lies in \mathcal{S} . Choosing both $\hat{q}_s \in \mathcal{S}$ and $\hat{x}_s \in \mathcal{S}$ for $\mathbf{s} = 0, 1$, we infer that $G_s^{\mathbb{C}}$ and G_s^{\ominus} are real-valued on \mathcal{S} for all $s \in [0, 1]$, since the bilinear form defined in (13) sends $\pi_K \mathcal{S} \times \pi_K \mathcal{S}$ to \mathbb{R} . We conclude that H_s maps \mathcal{S}_ν to $\mathcal{S}_{\nu'}$ for $1 < \nu' < \nu$.

Next, we choose the linear operators A_0 and A_1 such that they (and hence A_s for $s \in [0, 1]$) preserve symmetry in the sense that they leave \mathcal{S} invariant. This implies that T_s maps \mathcal{S} to itself for all $s \in [0, 1]$. To be explicit, for a linear operator $B = (B_{nm})$ on X we introduce the conjugate B^* as follows ($k, k' \in \mathbb{Z}$):

$$B_{nm}^* = \overline{B_{nm}} \quad \text{for } n, m = 1, \dots, M, \quad (37a)$$

$$(B_{nm}^*)_k = \overline{(B_{nm})_{-k}} \quad \text{for } m = 1, \dots, M, n = M + 1, \dots, M + N, \quad (37b)$$

$$(B_{nm}^*)_k = \overline{(B_{nm})_{-k}} \quad \text{for } n = 1, \dots, M, m = M + 1, \dots, M + N, \quad (37c)$$

$$(B_{nm}^*)_{k,k'} = \overline{(B_{nm})_{-k,-k'}} \quad \text{for } n, m = M + 1, \dots, M + N. \quad (37d)$$

Then $A_s, \mathbf{s} = 0, 1$ preserves conjugate symmetry if $A_s = A_s^*$.

Remark 4.1. *Since $i\mathbf{K}^{-1}$ preserves conjugate symmetry, conjugate symmetry preservation of A_s in practice reduces to symmetry preservation of the approximate numerical approximate inverse of $D\hat{H}_s(\hat{x}_s)$. Due to rounding error in computing the numerical inverse, this symmetry is not automatic. We therefore symmetrize the candidate inverse, denoted by \tilde{A}_s , through*

$$\hat{A}_s = \frac{\tilde{A} + \tilde{A}_s^*}{2},$$

with the conjugate defined in (37).

The symmetries thus allow us to conclude that the fixed point of T_s correspond to a *real*-valued periodic orbit of (1) under symmetry assumptions on the numerical data. In particular, in practice we fix some $K \in \mathbb{N}$ and choose

- the numerical approximate solutions \hat{x}_0 and \hat{x}_1 in $\Pi_K \mathcal{S}$;
- the numerical predictors $\hat{\dot{x}}_0$ and $\hat{\dot{x}}_1$ in $\Pi_K \mathcal{S}$;
- the phase condition parameters \hat{q}_0 and \hat{q}_1 in $\Pi_K \mathcal{S}$, see (17);
- conjugate symmetry preserving linear operators \hat{A}_0 and \hat{A}_1 , see Remark 4.1.

Theorem 4.2. *Let the symmetry assumptions on \hat{x}_s , $\hat{\dot{x}}_s$, \hat{q}_s , \hat{A}_s listed above be satisfied for $s = 0, 1$. Then, under the conditions of Theorem 3.1, the fixed point $x_{\text{sol}}(s) \in B_{\hat{r}}(x_s)$ of T_s is conjugate symmetric, i.e. $x_{\text{sol}}(s) \in \mathcal{S}$, for every $s \in [0, 1]$.*

Proof. Since \mathcal{S} is invariant under T_s and it intersects $B_{\hat{r}}(x_s)$, as $x_s \in \mathcal{S}$, the fixed point of T_s lies in $\mathcal{S} \cap B_{\hat{r}}(x_s)$. \square

Theorem 4.2 provides us with $x_{\text{sol}}(s) \in \mathcal{S}$, which we write as $x_{\text{sol}}(s) = ((\tau_{\text{sol}}, \mu_{\text{sol}}), v_{\text{sol}})(s)$. We have thus found a family of real-valued solutions

$$u_{\text{sol}}(t; s) \stackrel{\text{def}}{=} \sum_{k \in \mathbb{Z}} (v_{\text{sol}}(s))_k e^{ikt/\tau_{\text{sol}}(s)},$$

of (1) with period $L = 2\pi\tau_{\text{sol}}(s)$ at parameter value $\mu = \mu_{\text{sol}}(s) \in \mathbb{R}^{M-1}$. We denote

$$(1-s)\hat{x}_0 + s\hat{x}_1 = \hat{x}_s = (\hat{\lambda}_s, \hat{v}_s) = ((\hat{\tau}_s, \hat{\mu}_s), \hat{v}_s),$$

so that $x_s = \mathbf{E}\hat{x}_s \in \mathcal{S}$, see (15).

Remark 4.3. *Since $x_{\text{sol}}(s) \in B_{\hat{r}}(\mathbf{E}\hat{x}_s)$, the associated error estimates are*

$$\begin{aligned} \max_{t \in \mathbb{R}} \left| u_{\text{sol}}(t; s) - \hat{u}_s\left(\frac{\hat{\tau}_s}{\tau_{\text{sol}}(s)}t\right) \right|_{\infty} &\leq \hat{r}, \\ |\tau_{\text{sol}}(s) - \hat{\tau}_s| &\leq \hat{r}, \\ |\mu_{\text{sol}}(s) - \hat{\mu}_s|_{\infty} &\leq \hat{r}, \end{aligned} \tag{38}$$

for all $s \in [0, 1]$, where

$$\hat{u}_s(t) \stackrel{\text{def}}{=} \sum_{|k| \leq K} (\hat{v}_s)_k e^{ikt/\hat{\tau}_s}.$$

In particular, the bound (38) implies that for any $s \in [0, 1]$ the periodic orbit $u_{\text{sol}}(\cdot; s)$ lies within Hausdorff distance \hat{r} from the closed curve $\hat{u}_s(\cdot)$ in phase space (in the supremum norm).

5 Auxiliary estimates

In this section we collect some properties of operators on the space $X = \mathbb{C}^M \times (\ell_\nu^1)^N$ that will be used for the construction of the bounds. First, the dual of ℓ_ν^1 is the space ℓ_ν^∞ of bi-infinite sequences endowed with the supremum norm

$$\|y\|_\nu^\infty = \sup_{k \in \mathbb{Z}} \frac{|y_k|}{\nu^{|k|}}.$$

If $w \in \ell_\nu^1$ and $y \in \ell_\nu^\infty$, then

$$\left| \sum_{k \in \mathbb{Z}} y_k w_k \right| \leq \|w\|_\nu^\infty \|w\|_\nu.$$

The operator norm of a linear operator $Q : \ell_\nu^1 \rightarrow \ell_\nu^1$ that acts on $v \in \ell_\nu^1$ has

$$(Qv)_k = \sum_{k' \in \mathbb{Z}} Q_{kk'} v_{k'},$$

is given by

$$\|Q\|_{B(\ell_\nu^1, \ell_\nu^1)} = \sup_{k' \in \mathbb{Z}} \frac{1}{\nu^{|k'|}} \sum_{k \in \mathbb{Z}} |Q_{kk'}| \nu^{|k|}. \quad (39)$$

When considering a linear operator $Q : \ell_\nu^1 \rightarrow \ell_\nu^1$ such that $Q = \tilde{\Pi}_{K_1} Q \tilde{\Pi}_{K_2}$ for some $K_1, K_2 \in \mathbb{N}$, i.e. acting on a finite number of modes and returning a finite number of non-zero modes, then we will denote such operator with a superscript (F) . The operator norm of such an operator is computable:

$$\|Q^{(F)}\|_{B(\ell_\nu^1, \ell_\nu^1)} = \max_{|k'| \leq K_2} \frac{1}{\nu^{|k'|}} \sum_{|k| \leq K_1} |Q_{kk'}^{(F)}| \nu^{|k|}. \quad (40)$$

We will not make a distinction between the operator and the finite matrix that represents it.

In the estimates we will repeatedly encounter operators which decompose in a finite part (represented by a matrix) and a part that represents convolution with an element of $\tilde{\Pi}_{K_3} \ell_\nu^1$. The following lemma describes (with some slight generalization) how to bound the norm of such an operator.

Lemma 5.1. *Let $K_1, K_2, K_3 \in \mathbb{N}$. Let $Q^{(F)}$ be a $(2K_1 + 1) \times (2K_2 + 1)$ matrix with complex entries. Let y^* be a $(2K_3 + 1)$ vector with complex entries. Let $(y^{[k]})_{|k| > K_2}$ be a bi-infinite sequence of $(2K_3 + 1)$ vectors with*

$$|y_{k'}^{[k]}| \leq |y_{k'}^*|, \quad \text{for all } |k'| \leq K_3.$$

Let $Q : \ell_\nu^1 \mapsto \ell_\nu^1$ act on $v \in \ell_\nu^1$ by

$$(Qv)_k = \left(\tilde{E} Q^{(F)} \tilde{\Pi}_{K_2} v \right)_{k'} + \sum_{\substack{k=k'-K_3 \\ |k| > K_2}}^{k'+K_3} y_{k'-k}^{[k]} v_k, \quad \text{for } k' \in \mathbb{Z} \quad (41)$$

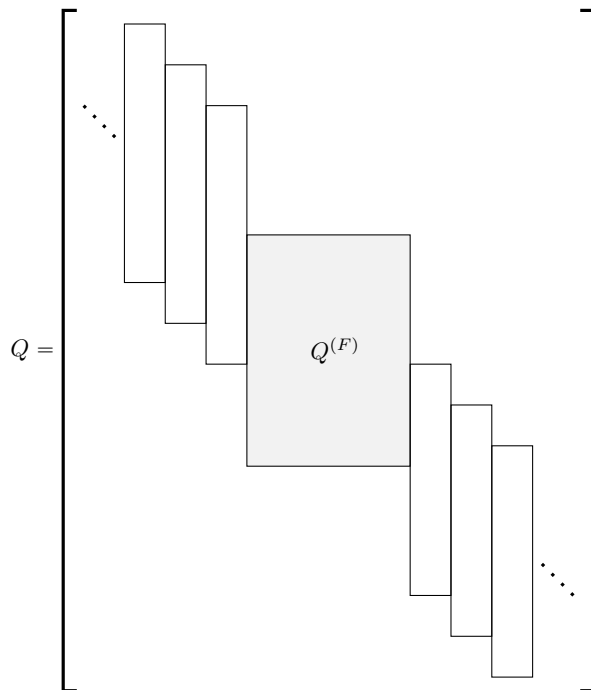


Figure 2: The shape of the operator Q , as defined in Lemma 5.1. The vertical columns represent the vectors $y^{[k]}$, where k denotes the column index.

i.e., Q has the form depicted in Figure 2. Then

$$\|Q\|_{B(\ell_\nu^1, \ell_\nu^1)} \leq \max(\|Q^{(F)}\|_{B(\ell_\nu^1, \ell_\nu^1)}, \|y^*\|_\nu).$$

The result also holds when Q has no “finite part” $Q^{(F)}$, *i.e.*, somewhat abusing notation, $K_2 = -1$.

Proof. A proof can be easily (re)constructed from [17, Corollary 1], where the special case $K_3 = 1$ is considered, of which Lemma 5.1 is a relatively straightforward extension. \square

We note that if $y^{[k]} = y^*$ for all k , then the final term in (41) corresponds to the convolution product $(y^*v)_k$.

In the remainder of this paper, we will make extensive use of the following lemma for the computation of norms of various operators from $X = \mathbb{C}^M \times (\ell_\nu^1)^N$ to itself. The proof is again standard and is thus omitted.

Lemma 5.2. *Let $B : X \rightarrow X$ be a linear operator which acts on $x \in X$ through the decomposition $\{B_{nm}\}_{1 \leq n, m \leq M+N}$ introduced in (25). Then the component-*

wise norms $\sup_{x \in B_1(0) \subset X} \|(Bx)_n\|$ satisfy, for $n = 1, \dots, M$,

$$\sup_{x \in B_1(0) \subset X} |(Bx)_n| \leq \sum_{m=1}^M |B_{nm}| + \sum_{m=M+1}^{M+N} \|B_{nm}\|_\nu^\infty,$$

while for $n = M + 1, \dots, M + N$ we have

$$\sup_{x \in B_1(0) \subset X} \|(Bx)_n\|_\nu \leq \sum_{m=1}^M \|B_{nm}\|_\nu + \sum_{m=M+1}^{M+N} \|B_{nm}\|_{B(\ell_\nu^1, \ell_\nu^1)}.$$

6 Validation of a single periodic orbit

For ease of exposition, in this section we present the explicit computation of the bounds introduced in Equations (30) and (31) for the case of a single solution. In Section 8 we generalize this to validated continuation of solution branches. The approximate numerical solution considered is denoted by $\hat{x} = (\hat{\lambda}, \hat{v})$, and the zero finding problem is of the form $H(x) = (G(x), F(x)) = 0$, with F and G defined in (6) and (20), respectively, are now *s-independent*.

6.1 Constructing the Newton-like operator T

In order to apply the radial polynomial approach to validate a numerical solution \hat{x} , we construct a Newton-like operation T by using A , the approximate inverse of $DH(\mathbf{E}\hat{x})$. The first step is the construction of A^\dagger , a (partly numerical) approximation of $DH(\mathbf{E}\hat{x})$, on which we will base our construction of A .

We split A and A^\dagger into a finite part, defined numerically and stored in the computer, and an infinite part, called the tail, defined analytically. The finite part of A^\dagger is chosen to be the finite dimensional Jacobian $D\hat{H}(\hat{x})$. The finite part of A is an numerically computed *approximate* inverse \hat{A} of $D\hat{H}(\hat{x})$, where \hat{H} is defined in (22). For the tail of A^\dagger the dominant term $\mathbf{i}k(v_n)_k$ is the natural candidate, while for the tail of A the corresponding choice is thus $\mathbf{i}k^{-1}(v_n)_k$.

To be precise, we define A and A^\dagger through

$$A^\dagger x \stackrel{\text{def}}{=} \mathbf{E} \left(D\hat{H}(\hat{x}) \Pi_K x \right) - \mathbf{i} \mathbf{K} \Pi_K^\infty x, \quad (42)$$

$$Ax \stackrel{\text{def}}{=} \mathbf{E} \left(\hat{A} \Pi_K x \right) - \mathbf{i} \mathbf{K}^{-1} \Pi_K^\infty x, \quad (43)$$

where

$$(\mathbf{K}x)_n \stackrel{\text{def}}{=} \begin{cases} 0 & \text{for } n = 1, \dots, M \\ \mathbf{k}x_n & \text{for } n = M + 1, \dots, M + N, \end{cases}$$

and

$$(\mathbf{K}^{-1}x)_n \stackrel{\text{def}}{=} \begin{cases} 0 & \text{for } n = 1, \dots, M \\ \mathbf{k}^{-1}x_n & \text{for } n = M + 1, \dots, M + N, \end{cases}$$

with (see also (28))

$$(\mathbf{k}w)_k \stackrel{\text{def}}{=} kw_k \quad \text{and} \quad (\mathbf{k}^{-1}w)_k \stackrel{\text{def}}{=} \begin{cases} 0 & \text{if } k = 0 \\ k^{-1}w_k & \text{if } k \in \mathbb{Z} \setminus \{0\}. \end{cases}$$

Remark 6.1. *The tails of A and A^\dagger are exact inverses, hence*

$$I - AA^\dagger = \mathbf{\Pi}_K - \mathbf{E}(\hat{A}D\hat{H}(\hat{x}))\mathbf{\Pi}_K, \quad (44)$$

i.e., $I - AA^\dagger$ is represented by a matrix.

Remark 6.2. *Since the tail of A is diagonal, when x has at most K' nonzero modes, then Ax has at most $\max\{K, K'\}$ nonzero modes.*

We note that A has the structure assumed in Lemma 5.1. Moreover, even though H does not map X into itself, we observe that $AH(x) \in X$ for all $x \in X$. In particular,

$$T : x \mapsto x - AH(x)$$

maps X to itself, cf. Proposition 4 in [17].

Having defined the fixed point operator T , we now derive explicit bounds Y and Z satisfying (30) and (46) in Sections 6.2 and 6.3, respectively.

6.2 The Y bound

In this section, we are interested in computing the Y bound, that is the $M + N$ vector such that

$$Y_n \geq \| [T(\mathbf{E}\hat{x}) - \mathbf{E}\hat{x}]_n \| = \| [AH(\mathbf{E}\hat{x})]_n \|, \quad \text{for } n = 1, \dots, M + N. \quad (45)$$

Since \hat{x} has K non-zero modes, by Remark 2.1 we know that $H(\mathbf{E}\hat{x})$ will have at most $K|D|$ non-zero modes (we recall that $|D|$ is the order of the polynomial vector field). Remark 6.2 implies that $AH(\mathbf{E}\hat{x})$ has at most $K|D|$ non-zero modes, all of which can be computed explicitly in a finite number of operations. By performing these operations with interval arithmetic we obtain bounds satisfying (45).

6.3 The splitting of the Z bound

In view of (31), the Z bound for the non-continuation case needs to satisfy

$$Z_n(r) \geq \sup_{b, c \in B_r(0)} \| [DT(\mathbf{E}\hat{x} + b)c]_n \|, \quad \text{for } n = 1, \dots, M + N. \quad (46)$$

We split the estimate into three parts:

$$\begin{aligned}
\sup_{b,c \in B_r(0)} \|[DT(\mathbf{E}\hat{x} + b)c]_n\| &\leq \underbrace{\sup_{c \in B_r(0)} \|[I - AA^\dagger]c\|_n}_{\leq Z_{0n}r} & (47) \\
&+ \underbrace{\sup_{c \in B_r(0)} \|[A(DH(\mathbf{E}\hat{x}) - A^\dagger)]c\|_n}_{\leq Z_{1n}r} \\
&+ \underbrace{\sup_{b,c \in B_r(0)} \|[A(DH(\mathbf{E}\hat{x}) - DH(\mathbf{E}\hat{x} + b))]c\|_n}_{\leq Z_{2n}(r)}, & (48)
\end{aligned}$$

where the first two parts are linear in r . We deal with the Z_{0n} , Z_{1n} and Z_{2n} bounds separately.

6.3.1 The Z_0 bound

Rescaling $c \rightarrow cr$, the Z_0 bounds have been defined as satisfying

$$Z_{0n} \geq \sup_{c \in B_1(0)} \|[I - AA^\dagger]c\|_n.$$

By using (44) we obtain

$$\begin{aligned}
\|[I - AA^\dagger]c\|_n &\leq \|[I - AA^\dagger]\mathbf{\Pi}_K c\| + \|[I - AA^\dagger]\mathbf{\Pi}_K^\infty c\|_n \\
&= \|\mathbf{(\Pi}_K - \mathbf{E}\hat{A}D\hat{H}(\hat{x})\mathbf{\Pi}_K)c\|_n.
\end{aligned}$$

Here $\mathbf{\Pi}_K - \mathbf{E}\hat{A}D\hat{H}(\hat{x})\mathbf{\Pi}_K$ can be represented as a finite matrix, hence we compute explicit bounds (6.3.1) by applying Lemma 5.2 and using (40).

6.3.2 The Z_1 bound

Rescaling $c \rightarrow cr$, we aim to find bounds of the form

$$Z_{1n} \geq \sup_{c \in B_1(0)} \|[A(A^\dagger - DH(\mathbf{E}\hat{x}))c]_n\|. \quad (49)$$

We first analyse the operator

$$B = A^\dagger - DH(\mathbf{E}\hat{x}).$$

It follows from the definition (42) of A^\dagger that $B_{nm} = 0$ for $n = 1, \dots, M$ and $m = 1, \dots, M + N$. Furthermore, for $n = M + 1, \dots, M + N$ and $m = 1, \dots, n$, we have that B_{nm} has at most $K|D|$ nonzero modes, and $\mathbf{\Pi}_K B_{nm} = 0$. Finally, it follows from (27) that

$$B_{nm} = \mathcal{T}_{\hat{f}_{n-M}^{e_m}(\mathbf{E}\hat{x})} - \tilde{\mathbf{\Pi}}_K \mathcal{T}_{\hat{f}_{n-M}^{e_m}(\mathbf{E}\hat{x})} \tilde{\mathbf{\Pi}}_K \quad \text{for } n, m = M + 1, \dots, M + N,$$

which has bandwidth at most $K(|D| - 1)$.

Remark 6.3. Before we proceed, consider the product $Q_1 Q_2$ of two operators in $B(\ell_\nu^1, \ell_\nu^1)$ of the form

$$\begin{aligned} Q_1 &= \tilde{\mathbf{E}} \hat{Q}_1 \tilde{\Pi}_K + i\mathbf{k}^{-1}(I - \tilde{\Pi}_K), \\ Q_2 &= \tilde{\mathbf{E}} \hat{Q}_2 \tilde{\Pi}_K + \mathcal{T}_y, \end{aligned}$$

for some $(2K+1) \times (2K+1)$ matrices \hat{Q}_1 and \hat{Q}_2 , and an element $y \in \ell_\nu^1$ with at most K' nonzero modes. Then the product $Q = Q_1 Q_2$ is of the form described in Lemma 5.1 with $K_1 = K + 2K'$, $K_2 = K + K'$ and $y^* = \frac{1}{K+1}y$, i.e. $K_3 = K'$.

For the product operator $AB = A(A^\dagger - DH(\mathbf{E}\hat{x}))$ we find that $(AB)_{nm} = 0$ for $n, m = 1, \dots, M$. Furthermore, $(AB)_{nm}$ has at most $K|D|$ nonzero modes for $n = 1, \dots, M$ and $m = M+1, \dots, M+N$, as well as for $n = M+1, \dots, M+N$ and $m = 1, \dots, M$. Finally, for $n, m = M+1, \dots, M+N$, based on Remark 6.3 we conclude that $(AB)_{nm}$ is of the form described in Lemma 5.1, with $K_1 = K|D|$, $K_2 = K(2|D| - 1)$ and $K_3 = K(|D| - 1)$ and $y_* = \frac{1}{K+1}|\hat{f}_{n-M}^{e_m}(\hat{x})|$.

We thus determine the bounds (49) explicitly by a direct computation based on Lemmas 5.2 and 5.1.

6.3.3 The Z_2 bound

The last bound is defined as satisfying

$$\tilde{Z}_{2n}(r) \geq \sup_{b, c \in B_r(0)} \| [A(DH(\mathbf{E}\hat{x}) - DH(\mathbf{E}\hat{x} + b))c]_n \|.$$

We apply the mean value theorem in Banach spaces:

$$\begin{aligned} & \sup_{b, c \in B_r(0)} \| (A[DH(\mathbf{E}\hat{x}) - DH(\mathbf{E}\hat{x} + b)]c)_n \| \\ & \leq \sup_{\bar{b}, \bar{c} \in B_1(0)} \sup_{\bar{z} \in B_1(0)} \| [A DDH(\mathbf{E}\hat{x} + \bar{z}r)\bar{b}\bar{c}]_n \| r^2 \\ & \leq \sup_{\bar{b}, \bar{c} \in B_1(0)} \sup_{\bar{z} \in B_1(0)} \sum_{m=1}^{M+N} \| A_{nm} \|_{B(X_n, X_m)} \| [DDH_m(\mathbf{E}\hat{x} + \bar{z}r)\bar{b}\bar{c}] \| r^2, \end{aligned}$$

with $\bar{b}r = b$ and $\bar{c}r = c$. The spaces X_n are defined in (26), and the operator norms $\|A_{nm}\|_{B(X_n, X_m)}$ can be computed directly (the ones on the diagonal tail, i.e. $n = m = M+1, \dots, M+N$, by using Lemma 5.1). The bound on

$$\| [DDH_m(\mathbf{E}\hat{x} + \bar{z}r)\bar{b}\bar{c}] \|$$

depends on r , but to simplify the computation we simply bound r a priori by some r_* , which in practice we choose to be large enough to safely assume it bigger than the validation radius. The inequality $r_* \geq r_{\max}$ for the interval of validation $\mathbf{I} = (r_{\min}, r_{\max})$ is checked at the end of the validation procedure.

We are thus looking for a bound on

$$\sup_{\bar{b}, \bar{c} \in B_1(0)} \sup_{z \in B_{r_*}(0)} \| [DDH_m(\mathbf{E}\hat{x} + z)\bar{b}\bar{c}] \| . \quad (50)$$

We start with $m = 1, \dots, M$. Both the phase condition and continuation equation are linear, hence $DDH_m = 0$ for $m = 1, 2$. For $m = 3, \dots, M$ the only non-vanishing terms in the derivative are

$$D^{e_n} D^{e_{n'}} H_m(\mathbf{E}\hat{x} + z) = D^{e_n + e_{n'}} \tilde{g}_{m-2}(\hat{\lambda} + z_\lambda) \quad \text{for } n, n' = 1, \dots, M.$$

where we have written $z = (z_\lambda, z_v)$. Each of these can be bounded uniformly for $z \in B_{r_*}(0)$ by using an interval arithmetic evaluation

$$J_{n,n',m} = |D^{e_n + e_{n'}} \tilde{g}_{m-2}(\hat{\lambda}_{r_*})|$$

where $\hat{\lambda}_{r_*}$ is the product of intervals $\prod_{j=1}^M [\hat{\lambda}_j - r_*, \hat{\lambda}_j + r_*]$. Hence, for $m = 1, \dots, M$ the expression (50) is bounded by

$$\mathcal{Z}_m := \begin{cases} 0 & \text{for } m = 1, 2 \\ \sum_{n,n'=1}^M \max J_{n,n',m} & \text{for } m = 3, \dots, M. \end{cases}$$

Next we consider $m = M + 1, \dots, M + N$, for which we have

$$\begin{aligned} D^{e_n} D^{e_{n'}} H_m(\mathbf{E}\hat{x} + z) &= \hat{f}_{m-M}^{e_n + e_{n'}}(\mathbf{E}\hat{x} + z) \\ &= \sum_{\beta \in \mathcal{D}(e_n + e_{n'}, m-M)} \tilde{f}_{\beta, e_n + e_{n'}, m-M}(\hat{\lambda} + z_\lambda) \prod_{i=1}^N (\mathbf{E}\hat{v}_i + (z_v)_i)^{\beta_i}, \end{aligned} \tag{51}$$

where we have used the identification (of derivatives) based on convolution multiplication introduced in Remark 2.6. We estimate these convolution polynomials term by term with the help of the Banach algebra property (9). Each monomial in (51) is bounded in norm by

$$\tilde{J}_{\beta, n, n', m} := |\tilde{f}_{\beta, e_n + e_{n'}, m-M}(\hat{\lambda}_{r_*})| \prod_{j=1}^N (\|\hat{v}_j\|_\nu + r_*)^{\beta_j},$$

which is to be evaluated in an interval arithmetic sense. Using once again the Banach algebra property and the triangle inequality, this leads to the following bounds on (50) for $m = M + 1, \dots, M + N$:

$$\mathcal{Z}_m = \sum_{n,n'=1}^{M+N} \sum_{\beta \in \mathcal{D}(e_n + e_{n'}, m-M)} \max \tilde{J}_{\beta, n, n', m}.$$

Finally, we set $\tilde{Z}_{2n}(r) := Z_{2n} r^2$ with

$$Z_{2n} := \sum_{m=1}^{M+N} \|A_{nm}\|_{B(X_n, X_m)} \mathcal{Z}_m.$$

6.4 Conclusion

Once we have computed all the bounds in this section, we construct the radii polynomials

$$p_n(r) = Y_n + (Z_{0n} + Z_{1n})r - r + Z_{2n}r^2.$$

If there exists an $r \leq r_*$ for which all p_n are negative, then applying Theorem 3.1 guarantees the existence of a fixed point contraction and, therefore, of a periodic orbit satisfying the error bounds listed in Remark 4.3. The proof of injectivity of A is discussed in Section 8.5 in the more general context of continuation.

An advantage of using the mean value theorem in Section 6.3.3 is that, irrespective of the order of the vector field, the radii polynomials are always of order 2. The approach taken in, for example, [5] and [17] leads to $Z_2(r)$ bounds whose order depends on the order of the vector field. Our bounds are slightly less sharp due to our central goal of universal applicability, and they remain sufficiently effective in practice.

7 Examples: single solutions

Before we move on to continuation in Section 8, in this section we present some results on single orbit validation. We use the well-known van der Pol equation

$$\begin{cases} \dot{u}_1 = u_2, \\ \dot{u}_2 = \mu u_2 - \mu u_1^2 u_2 - u_1, \end{cases} \quad (52)$$

to discuss proper choices for the computational parameters ν and K in rigorous single orbit validation. The system (52) has a unique attracting limit cycle for any $\mu > 0$. In the limit $\mu \downarrow 0$ it tends to a circle in phase space and is essentially described by a single Fourier mode. For large μ its dynamics fall in the fast-slow paradigm and more and more Fourier modes are required to describe the orbit accurately.

We first fix $\mu = 1.1$ and investigate the dependence on ν and K . For various choices of $\nu > 1$, in Figure 3 we depict the dependence on K of the validation interval (r_{\min}, r_{\max}) on which all radii polynomials are negative. As expected, we see that for small K validation fails. For K between roughly 20 and 50 the validation interval grows. For ν sufficiently close to 1 it then stabilizes for $K > 50$, whereas for larger values of ν it starts to decrease again when K increases. The latter is due to the large weights in the ℓ_ν^1 norm in that case, which may be viewed as a computational instability of the method. Indeed, the Fourier coefficients of the solution decay at some (unknown) rate $\nu_{\text{sol}} > 1$. In theory, for any choice $\nu \in (1, \nu_{\text{sol}})$ the method should lead to validation for large K , but this is hampered by the finite precision of floating point numbers. For larger values of ν these rounding errors lead to instability for large K . The main conclusion is that it is prudent to choose ν sufficiently close to unity.

We then fix $\nu = 1.02$ and vary μ to see how the minimal number of Fourier modes needed to describe a validated solution increases as the complexity of the

solution increases. The results are shown in Figure 4. The smallest μ chosen here is $\mu = 10^{-4}$. For μ even closer to 0 ($\mu < 10^{-8}$), we cannot validate the solution, since it loses its isolation property as it merges into a one parameter family for $\mu = 0$. For large μ the large number of modes needed to properly describe and validate the solution leads to more and more time and memory requirements. This is illustrated in Figure 5, where the computational time is plotted versus the number of modes used. The dominant cost is in the matrix-matrix product(s) in the Z_1 bound, see Section 6.3.2. The cubic growth $O(K^3)$ is thus not unexpected.

Next, to study the dependence on the size of the system we look at the generalization

$$\begin{cases} \dot{u}_1 = u_2, \\ \dot{u}_i = (1 - u_1^2) \frac{u_i + u_{i+1}}{2} - u_i, \quad \text{for } i = 2, \dots, N. \end{cases} \quad (53)$$

where $u_{N+1} = u_2$. It is easily seen that the u_i are all equal for $i \geq 2$, but the computation does not take advantage of this fact. We note that the validation interval does not depend significantly on N in this example. This is in part due to the choice of the maximum norm in (10), which prevents errors in different components from accumulating. In Figure 6 we plot the computational time versus the size of the system. We conclude that the time (for fixed $K = 50$) grows roughly as $O(N^3)$ due to the aforementioned matrix-matrix product being in the computation of the Z_1 bound being the bottle neck.

The computational time also depends on the order of the polynomial. We select the generalization

$$\begin{cases} \dot{u}_1 = u_2, \\ \dot{u}_2 = \mu u_2 - \mu u_1^2 u_2 - u_1 + \epsilon_D u_1^D, \end{cases} \quad (54)$$

as our example, where we set $\mu = 1$. Since the size of u_1 is roughly 2, we choose $\epsilon_D = \frac{1}{10} 2^{-D}$ to prevent excessive growth of the D -dependent term. In Figure 7 we plot the computational time versus the order D . The cubic dependence is due to the size of the matrices involved in the Z_1 bound growing linearly in D , see Section 6.3.2. We remark that the code is suboptimal in this respect, as in the products $(AB)_{nm}$ we did not take advantage of the fact that A is sparse for large D , since it has a long diagonal tail. There is clearly room for improvement here; quadratic growth in D should be achievable.

As a final illustration, see Figure 8, we have verified a single long periodic orbit in the Lorenz system (using classical notation rather than the general notation from (1))

$$\begin{cases} \dot{x} = \sigma(y - x), \\ \dot{y} = x(\rho - z) - y, \\ \dot{z} = xy - \beta z, \end{cases} \quad (55)$$

where $\sigma = 10$, $\beta = 8/3$ and $\rho = 28$. Here we used $\nu = 1 + 10^{-6}$ and $K = 800$.

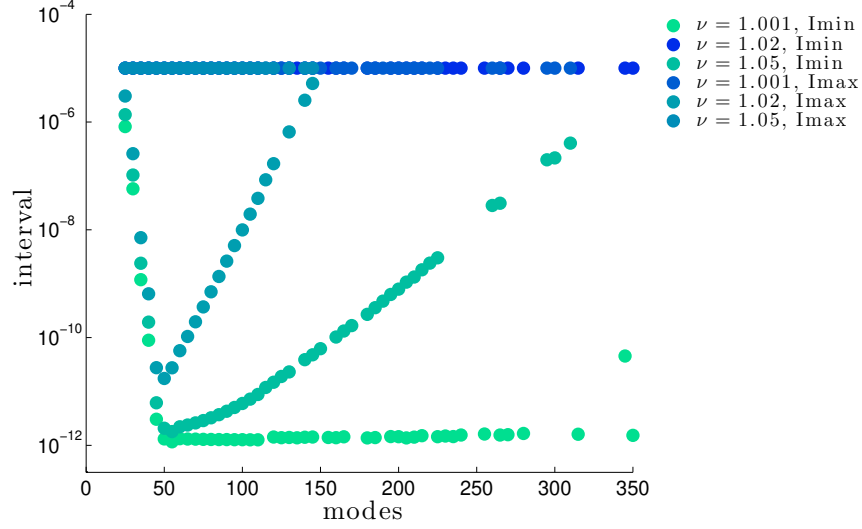


Figure 3: The boundaries of the validation interval (r_{\min}, r_{\max}) versus the number of modes K for various values of ν .

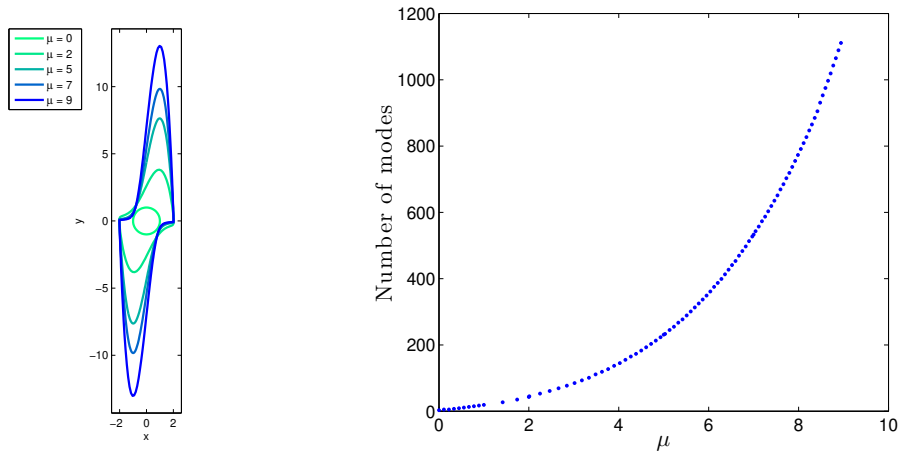


Figure 4: On the right: the minimal number of modes K necessary for the validation of a periodic orbit of (52) depending on μ . The stepsize in μ is not chosen uniformly, because the problem is more sensitive to changes in μ for μ bigger, therefore requesting a steeper change in the number of modes. On the left: several of the validated periodic orbits..

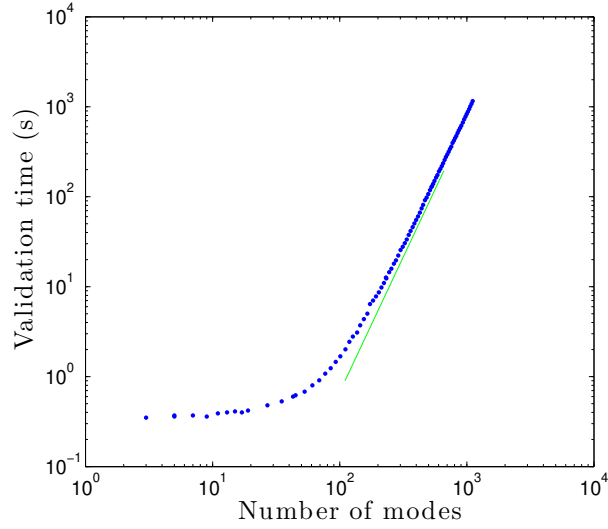


Figure 5: The computation time versus the number of modes K . The reference line has a slope corresponding to K^3 .

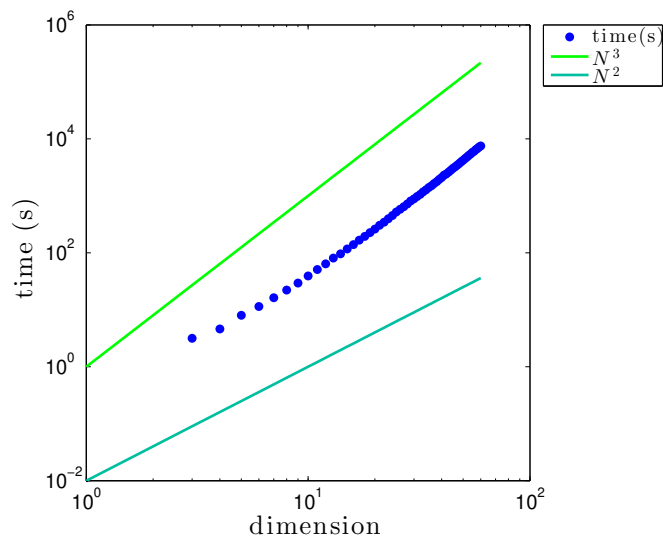


Figure 6: The computation time versus the dimension N of the system (53). The reference lines have slopes corresponding to quadratic and cubic dependence on N .

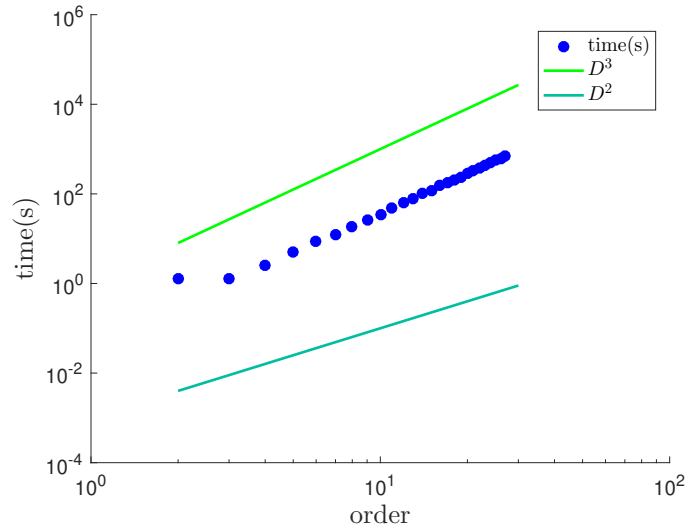


Figure 7: The computation time versus the order D of the system (54). The reference lines have slopes corresponding to quadratic and cubic dependence on D .

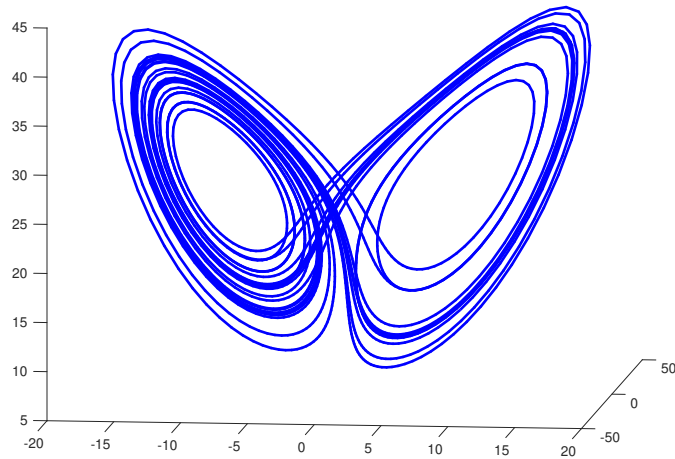


Figure 8: Validation of a periodic solution for the Lorenz system (55) with the classical parameter values $\sigma = 10$, $\beta = 8/3$ and $\rho = 28$. The solution has a period close to 25. This solution was validated with $\nu = 1 + 10^{-6}$ and $K = 800$

8 Rigorous curve following

8.1 Interpolation bounds

In Section 6 we presented bounds to validate single periodic orbits. In this Section we extend those results to the case of continuation. We will be referring extensively to the results presented in Section 6 and combine these with the following interpolation lemma.

Lemma 8.1. *Let $h : [0, 1] \mapsto \mathbb{C}$ be C^2 , then*

$$\max_{s \in [0,1]} |h(s)| \leq \max\{|h(0)|, |h(1)|\} + \frac{1}{8} \max_{s \in [0,1]} |h''(s)|. \quad (56)$$

Proof. The result is classical for real-valued functions. For the complex case we argue as follows. Let $M \stackrel{\text{def}}{=} \max_{s \in [0,1]} |h''(s)|$. Define

$$\tilde{h}(s) \stackrel{\text{def}}{=} h(s) - [(1-s)h(0) + sh(1)],$$

then $\tilde{h}(0) = 0$ and $\tilde{h}(1) = 0$. Furthermore, $M = \max_{s \in [0,1]} |\tilde{h}''(s)|$. We will show that

$$\max_{s \in [0,1]} |\tilde{h}(s)| \leq \frac{1}{8} M. \quad (57)$$

The result on h follows by using the triangle inequality and convexity of the modulus:

$$\max_{s \in [0,1]} |h(s)| \leq \max_{s \in [0,1]} |(1-s)h(0) + sh(1)| + \max_{s \in [0,1]} |\tilde{h}(s)| \leq \max\{|h(0)|, |h(1)|\} + \frac{M}{8}.$$

To prove (57) we argue as follows. Let the maximum $\max_{s \in [0,1]} |\tilde{h}(s)|$ be attained in $s = s_0$. If $|\tilde{h}(s_0)| = 0$ then $\tilde{h} \equiv 0$ and there is nothing left to prove. For $|\tilde{h}(s_0)| > 0$ we assume, without loss of generality, that $\frac{1}{2} \leq s \leq 1$ (reparametrizing $s \rightarrow 1-s$ if necessary). We split \tilde{h} into real and imaginary part: $\tilde{h} = \tilde{h}_r + i\tilde{h}_i$. Then $\tilde{h}_r(s_0)\tilde{h}'_r(s_0) + \tilde{h}_i(s_0)\tilde{h}'_i(s_0) = 0$. Consider the real-valued function $\hat{h}(s) \stackrel{\text{def}}{=} \tilde{h}_r(s_0)\tilde{h}_r(s) + \tilde{h}_i(s_0)\tilde{h}_i(s)$. We have $\hat{h}(s_0) = |\tilde{h}(s_0)|^2$ and $\hat{h}'(s_0) = 0$. For the second derivative it follows from the Cauchy-Schwarz inequality that for all $s \in [0, 1]$

$$|\hat{h}''(s)| = |\tilde{h}_r(s_0)\tilde{h}''_r(s) + \tilde{h}_i(s_0)\tilde{h}''_i(s)| \leq |\tilde{h}(s_0)| |\tilde{h}''(s)| \leq M |\tilde{h}(s_0)|. \quad (58)$$

Furthermore, $\hat{h}(1) = 0$. By Taylor's theorem we may write, for some $\xi \in (s_0, 1)$,

$$\begin{aligned} 0 = \hat{h}(1) &= \hat{h}(s_0) + \hat{h}'(s_0) + \frac{(1-s_0)^2}{2} \hat{h}''(\xi) \\ &\geq |\tilde{h}(s_0)|^2 - \frac{1}{8} M |\tilde{h}(s_0)|, \end{aligned}$$

where the inequality follows from (58). We conclude that $|\tilde{h}(s_0)| \leq \frac{M}{8}$, which proves (57) since the maximum is attained in s_0 . \square

For $w, w' \in \ell_\nu^1$ we denote by $|w| \in \ell_\nu^1$ the elementwise absolute value and by $\max\{w, w'\} \in \ell_\nu^1$ the elementwise maximum.

Lemma 8.2. *Let $w : [0, 1] \rightarrow \ell_\nu^1$ be C^2 , then*

$$\max_{s \in [0, 1]} \|w(s)\|_\nu \leq \| \max\{|w(0)|, |w(1)|\} \|_\nu + \frac{1}{8} \left\| \max_{s \in [0, 1]} |w''(s)| \right\|_\nu.$$

Proof. We note that the ℓ_ν^1 norm has the property

$$\max_{s \in [0, 1]} \|w(s)\|_\nu \leq \| \max_{s \in [0, 1]} |w(s)| \|_\nu.$$

The assertion now follows by applying Lemma 8.1 elementwise and using the triangle inequality. \square

A similar result holds for $\tilde{w} : [0, 1] \rightarrow (\ell_\nu^1)^* \cong \ell_\nu^\infty$, with the same conventions for $|\tilde{w}|$ and $\max\{\tilde{w}, \tilde{w}'\}$.

Lemma 8.3. *Let $\tilde{w} : [0, 1] \rightarrow (\ell_\nu^1)^*$ be C^2 , then*

$$\max_{s \in [0, 1]} \|\tilde{w}(s)\|_\nu^\infty \leq \| \max\{|\tilde{w}(0)|, |\tilde{w}(1)|\} \|_\nu^\infty + \frac{1}{8} \left\| \max_{s \in [0, 1]} |\tilde{w}''(s)| \right\|_\nu^\infty.$$

For $Q, Q' \in B(\ell_\nu^1, \ell_\nu^1)$ we denote by $|Q| \in B(\ell_\nu^1, \ell_\nu^1)$ the elementwise absolute value, i.e.,

$$(|Q|w)_k = \sum_{k' \in \mathbb{Z}} |Q_{kk'}| w_{k'}.$$

Similarly, by $\max\{Q, Q'\} \in B(\ell_\nu^1, \ell_\nu^1)$ we denote the elementwise maximum.

Lemma 8.4. *Let $Q : [0, 1] \rightarrow B(\ell_\nu^1, \ell_\nu^1)$ be C^2 then*

$$\max_{s \in [0, 1]} \|Q(s)\|_{B(\ell_\nu^1, \ell_\nu^1)} \leq \| \max\{|Q(0)|, |Q(1)|\} \|_{B(\ell_\nu^1, \ell_\nu^1)} + \frac{1}{8} \left\| \max_{s \in [0, 1]} |Q''(s)| \right\|_{B(\ell_\nu^1, \ell_\nu^1)}.$$

Proof. We note that it follows from the formula (39) for the operator norm that

$$\max_{s \in [0, 1]} \|Q(s)\|_{B(\ell_\nu^1, \ell_\nu^1)} \leq \| \max_{s \in [0, 1]} |Q(s)| \|_{B(\ell_\nu^1, \ell_\nu^1)}.$$

The assertion now follows by applying Lemma 8.1 elementwise and using the triangle inequality. \square

8.2 Constructing the Newton-like operator T_s

We recall that starting from two numerically obtained approximate zeros \hat{x}_0 and \hat{x}_1 , we set out to find solutions of $H_s(x) = 0$ in a cylinder around the line segment

$$x_s \stackrel{\text{def}}{=} \mathbf{E} \hat{x}_s \stackrel{\text{def}}{=} \mathbf{E}[(1-s)\hat{x}_0 + s\hat{x}_1],$$

which consists of elements with at most K nonzero modes. For later use we introduce

$$x_\Delta \stackrel{\text{def}}{=} x_1 - x_0.$$

We note that the only equations that depend explicitly on s are the continuation equation $G_s^\circ = 0$ and the phase condition $G_s^\mathbb{C} = 0$. Furthermore, it follows directly from their definitions in (19) and (18) that

$$G_s^\circ(x_s) = 0 \quad \text{and} \quad G_s^\mathbb{C}(x_s) = 0 \quad \text{for all } s \in [0, 1].$$

To define the interpolated fixed point operator, we start by introducing the operators A_0^\dagger , A_1^\dagger , A_0 and A_1 , which are defined as in (42) and (43), with H replaced by H_0 and H_1 and \hat{x} by \hat{x}_0 and \hat{x}_1 , respectively:

$$\begin{aligned} A_0^\dagger x &= \mathbf{E} D \hat{H}_0(\hat{x}_0) \Pi_K x - \mathbf{i} \mathbf{K} I_K x, & A_1^\dagger y &= \mathbf{E} D \hat{H}_1(\hat{x}_1) \Pi_K x - \mathbf{i} \mathbf{K} I_K x, \\ A_0 x &= \mathbf{E} \hat{A}_0 \Pi_K x - \mathbf{i} \mathbf{K}^{-1} I_K x, & A_1 x &= \mathbf{E} \hat{A}_1 \Pi_K x - \mathbf{i} \mathbf{K}^{-1} I_K x, \end{aligned}$$

with $\hat{A}_s \approx (DH_s(\hat{x}_s))^{-1}$ for $s = 0, 1$. We define

$$A_s^\dagger \stackrel{\text{def}}{=} (1-s)A_0^\dagger + sA_1^\dagger \quad \text{and} \quad A_s \stackrel{\text{def}}{=} (1-s)A_0 + sA_1,$$

as well as

$$A_\Delta^\dagger \stackrel{\text{def}}{=} A_1^\dagger - A_0^\dagger, \quad \text{and} \quad A_\Delta \stackrel{\text{def}}{=} A_1 - A_0.$$

Remark 8.5. Both A_Δ^\dagger and A_Δ have just a finite nontrivial part since the tails vanish, e.g.

$$A_\Delta x = \mathbf{E}(\hat{A}_1 - \hat{A}_0) \Pi_K x.$$

With T_s defined in (29), we now derive explicit bounds Y and Z satisfying (30) and (46) in Sections 8.3 and 8.4, respectively.

8.3 The Y bound

We are looking for bounds $Y \in \mathbb{R}^{N+M}$ that satisfies

$$Y_n \geq \max_{s \in [0,1]} \|[A_s H_s(x_s)]_n\|, \quad \text{for } n = 1, \dots, M+N.$$

Since x_s has at most K non-zero modes, we argue as in Section 6.2 to conclude that $A_s H_s(x_s)$ has at most $K|D|$ non-zero modes for all $s \in [0, 1]$.

Remark 8.6. Indicating the explicit dependence of a function $P_s(x)$ on s by subscript s , we denote by $\partial_s P_s$ the partial derivative with respect to s , by DP_s the derivative with respect to x , and by $D_s P_s$ the total derivative

$$D_s P_s(x_s) = \partial_s P_s(x_s) + DP(x_s) x_\Delta.$$

By applying Lemma 8.1 for $n = 1, \dots, M$ and Lemma 8.2 for $n = M + 1, \dots, M + N$ it follows that

$$\begin{aligned} \max_{s \in [0,1]} \| [A_s H_s(x_s)]_n \| \leq \frac{1}{8} \underbrace{\left\| \max_{s \in [0,1]} [D_s D_s(A_s H_s(x_s))]_n \right\|}_{Y_{\Delta,n}} \\ + \underbrace{\left\| \max \{ |(A_0 H_0(\hat{x}_0))_n|, |(A_1 H_1(\hat{x}_1))_n| \} \right\|}_{Y_{0,n}}. \end{aligned} \quad (59)$$

The second part of the righthand side in (59) is very similar to the computations already presented in the single orbit scenario in Section 6.2, modulo the maximum and the absolute values (elementwise for $n = M + 1, \dots, M + N$). Indeed, the interval arithmetic computation of

$$Y_{0,n} = \left\| \max \{ |(A_0 H_0(\hat{x}_0))_n|, |(A_1 H_1(\hat{x}_1))_n| \} \right\|$$

takes a finite number of operations.

Concerning the first term in the righthand side of (59) we start by noting that the simple (linear) explicit dependence of H_s on s implies that

$$\partial_s H_s(x) = H_{\Delta}(x) \stackrel{\text{def}}{=} \begin{pmatrix} G_1^{\circ}(x) - G_0^{\circ}(x) \\ G_1^{\circ}(x) - G_0^{\circ}(x) \\ 0 \\ 0 \end{pmatrix}.$$

We then expand

$$D_s D_s(A_s H_s(x_s)) = 2A_{\Delta} D H(x_s) x_{\Delta} + A_s D D H(x_s) x_{\Delta} x_{\Delta} \quad (60)$$

$$+ 2A_{\Delta} H_{\Delta}(x_s) + 2A_s D H_{\Delta}(x_s) x_{\Delta}, \quad (61)$$

where we have used that A_s is linear in s . Since both x_s and x_{Δ} have at most K nonzero modes, both $D H(x_s) x_{\Delta}$ and $D D H(x_s) x_{\Delta} x_{\Delta}$ have at most $K|D|$ nonzero modes. Since A_{Δ} has a non-vanishing finite part only, and A_s is diagonal, the righthand side of (60) also has at most $K|D|$ nonzero modes. To compute, we replace $x_s = (\lambda_s, v_s)$ by an interval-valued variable $\mathcal{I}_{\hat{x}_s} = (\mathcal{I}_1^{\lambda}, \dots, \mathcal{I}_M^{\lambda}, \mathcal{I}_1^v, \dots, \mathcal{I}_N^v)$, where

$$\mathcal{I}_j^{\lambda} = [\min\{(\hat{\lambda}_0)_j, (\hat{\lambda}_1)_j\}, \max\{(\hat{\lambda}_0)_j, (\hat{\lambda}_1)_j\}], \quad (62)$$

$$(\mathcal{I}_i^v)_k = [\min\{(\hat{v}_0)_i, (\hat{v}_1)_i\}_k, \max\{(\hat{v}_0)_i, (\hat{v}_1)_i\}_k], \quad (63)$$

for $|k| \leq K$, whereas $(\mathcal{I}_i^v)_k = 0$ for $|k| > K$. In a similar way we replace each element of the finite part $(1-s)\hat{A}_0 + s\hat{A}_1$ of A_s by an interval with the relevant elements of \hat{A}_0 and \hat{A}_1 as its endpoints. We note that the tail of A_s does not depend on s . The resulting operator, consisting of a finite matrix of intervals and diagonal tails given by $i\mathbf{K}^{-1}I_K$, is denoted by \mathcal{A}_s . The terms in (61) can

be dealt with analogously. We conclude that it takes a finite interval arithmetic computation to enclose all non-vanishing components of

$$\mathcal{Y}_n \stackrel{\text{def}}{=} [2A_\Delta DH(\mathcal{I}_{\hat{x}_s})x_\Delta]_n + [A_s DDH(\mathcal{I}_{\hat{x}_s})x_\Delta x_\Delta]_n \\ + [2A_\Delta H_\Delta(\mathcal{I}_{\hat{x}_s})]_n + [2A_s DH_\Delta(\mathcal{I}_{\hat{x}_s})x_\Delta]_n,$$

for $n = 1, \dots, M + N$. We then set

$$Y_{\Delta,n} = \uparrow \max_{s \in [0,1]} \|\mathcal{Y}_n\|,$$

where the \uparrow denotes taking the maximum of the interval which results from the interval arithmetic computation. We will take similar maxima of intervals which result from interval arithmetic computations throughout without expression this in the notation.

8.4 The $Z(r)$ bound

The $Z(r)$ bounds consist of bounds on the derivative of the operator T_s in a ball of radius r , uniform for $s \in [0, 1]$. More precisely, the $Z_n(r)$ component of the radii polynomial is a bound on

$$\max_{s \in [0,1]} \sup_{b, c \in B_r(0) \subset X} \|[DT_s(x_s + b)c]_n\| = \sup_{s, b, c} \|[(I - A_s DH_s(x_s + b))c]_n\|.$$

We perform the same splitting as in Section 6:

$$\begin{aligned} \sup_{s, b, c} \|[(I - A_s DH_s(x_s + b))c]_n\| &\leq \underbrace{\sup_{s, b, c} \|[(I - A_s A_s^\dagger)c]_n\|}_{\leq Z_{0n}r} \\ &\quad + \underbrace{\sup_{s, b, c} \|[A_s [A_s^\dagger - DH_s(x_s)]c]_n\|}_{\leq Z_{1n}r} \\ &\quad + \underbrace{\sup_{s, b, c} \|[A_s [DH_s(x_s) - DH_s(x_s + b)]c]_n\|}_{\leq Z_{2n}(r)}. \end{aligned} \tag{64}$$

Each of these three bounds will be considered separately.

8.4.1 The Z_0 bound

Rescaling $c \rightarrow cr$ we set out to estimate

$$\sup_{s \in [0,1]} \sup_{c \in B_1(0)} \|[(I - A_s A_s^\dagger)c]_n\| r.$$

We apply Lemma 5.2 to obtain the estimate

$$\sup_{c \in B_1(0)} \|[(I - A_s A_s^\dagger)c]_n\| \leq \sum_{m=1}^{M+N} \|(I - A_s A_s^\dagger)_{nm}\|,$$

where the norm on the lefthand side is in X_n , while the operator norm on the right is in $B(X_m, X_n)$. It follows from the definition of A_s and A_s^\dagger that

$$I - A_s A_s^\dagger = \mathbf{E}[\Pi_K - ((1-s)D\hat{A}_0 + s\hat{A}_1)((1-s)D\hat{H}_0(\hat{x}_0) + sD\hat{H}_1(\hat{x}_1))\Pi_K],$$

hence the operator is represented by a finite (s -dependent) matrix. Omitting \mathbf{E} and Π_K from the notation, and setting $\hat{A}_s^\dagger = D\hat{H}_s(\hat{x}_s)$ for $s = 0, 1$, we write

$$I - A_s A_s^\dagger = (1-s)(\hat{I} - \hat{A}_0 \hat{A}_0^\dagger) + s(\hat{I} - \hat{A}_1 \hat{A}_1^\dagger) - s(1-s)(\hat{A}_1 - \hat{A}_0)(\hat{A}_1^\dagger - \hat{A}_0^\dagger),$$

where \hat{I} is the identity matrix on $\mathbb{C}^{M+(2K+1)N}$. Next, we apply Lemma 8.1 for any $n, m = 1, \dots, M$, Lemma 8.2 for $n = 1, \dots, M$ and $m = M+1, \dots, M+N$, Lemma 8.3 for $n = M+1, \dots, M+N$ and $m = 1, \dots, M$, and Lemma 8.4 for $n, m = M+1, \dots, M+N$ to obtain, uniformly for $s \in [0, 1]$,

$$\begin{aligned} \|(I - A_s A_s^\dagger)_{nm}\| &\leq \frac{1}{4} \left\| \|((\hat{A}_1 - \hat{A}_0)(\hat{A}_1^\dagger - \hat{A}_0^\dagger))_{nm}\| \right\| \\ &\quad + \left\| \max \left\{ |(I - \hat{A}_0 \hat{A}_0^\dagger)_{nm}|, |(I - \hat{A}_1 \hat{A}_1^\dagger)_{nm}| \right\} \right\|. \end{aligned} \quad (65)$$

We recall that absolute values and the maximum are to be interpreted element-wise. Since each of these is represented by a scalar, a finite vector or a matrix, the norms in the righthand side of (65) can be computed explicitly (e.g. via (40) for the matrices).

8.4.2 The Z_1 bound

We start the estimate analogously to Section 8.4.1, namely

$$\max_{s \in [0,1]} \sup_{c \in B_r(0)} \|[A_s(A_s^\dagger - DH_s(x_s))c]_n\| \leq r \sum_{m=1}^{M+N} \max_{s \in [0,1]} \|(A_s[A_s^\dagger - DH_s(x_s)])_{nm}\|.$$

By applying Lemmas 8.1-8.4 (as in Section 8.4.1) we infer that

$$\begin{aligned} \|(A_s[A_s^\dagger - DH_s(x_s)])_{nm}\| &\leq \frac{1}{8} \left\| \max_{s \in [0,1]} |D_s D_s (A_s(A_s^\dagger - DH_s(x_s)))_{nm}| \right\| \\ &\quad + \left\| \max \left\{ |(A_0(A_0^\dagger - DH_0(x_0)))_{nm}|, |(A_1(A_1^\dagger - DH_1(x_1)))_{nm}| \right\} \right\|, \end{aligned} \quad (66)$$

uniformly for $s \in [0, 1]$.

With regard to the second term, we argue as in Section 6.3.2. For both $s = 0$ and $s = 1$ the product $\Gamma_{nm}^s = (A_s(A_s^\dagger - DH_s(x_s)))_{nm}$ has the following properties. We have $\Gamma_{nm}^s = 0$ for $n, m = 1, \dots, M$. Furthermore, Γ_{nm}^s has at most $K|D|$ nonzero modes for $n = 1, \dots, M$ and $m = M+1, \dots, M+N$, as well as for $n = M+1, \dots, M+N$ and $m = 1, \dots, M$. Finally, for $n, m = M+1, \dots, M+N$, based on Remark 6.3 we conclude that Γ_{nm}^s is of the form described in Lemma 5.1, with $K_1 = K|D|$, $K_2 = K(2|D| - 1)$ and

$K_3 = K(|D| - 1)$ and $y_* = \frac{1}{K+1}|\widehat{f}_{n-M}^{e_m}(\hat{x}_i)|$. The operator $\tilde{\Gamma}$, consisting of the elementwise maxima

$$\tilde{\Gamma}_{nm} = \max\{ |(\Gamma^0)_{nm}|, |(\Gamma^1)_{nm}| \},$$

has these same properties, now with $y_* = \frac{1}{K+1} \max\{ |\widehat{f}_{n-M}^{e_m}(\hat{x}_0)|, |\widehat{f}_{n-M}^{e_m}(\hat{x}_1)| \}$, where also this maximum is to be interpreted elementwise. The norms $\|\tilde{\Gamma}_{nm}\|$ for $n, m = 1, \dots, M + N$ can thus be estimated explicitly by a direct computation based on Lemmas 5.2 and 5.1.

Next we consider the first term in the righthand side of (66). We expand

$$D_s D_s (A_s (A_s^\dagger - DH_s(x_s)))_{nm} = 2(A_\Delta A_\Delta^\dagger)_{nm} \quad (67)$$

$$- 2(A_\Delta \partial_s DH_s(x_s) x_\Delta)_{nm} \quad (68)$$

$$- 2(A_\Delta DDH_s(x_s) x_\Delta)_{nm} \quad (69)$$

$$- (A_s DDDH_s(x_s) x_\Delta x_\Delta)_{nm}. \quad (70)$$

We start by considering each of the four terms separately and then we gather them.

The first one (in (67)) has a finite part only, i.e. a vanishing tail, hence it can be computed explicitly with interval arithmetic.

In the second one (i.e. (68)) the factor $(\partial_s DH_s(x_s) x_\Delta)_{lm}$ has non-vanishing components only for $l = 1, 2$ and these again have a finite part only, hence they can be enclosed explicitly using interval arithmetic after replacing x_s by $\mathcal{I}_{\hat{x}_s}$, see(62) and (63).

In the third one (i.e. (69)) the factor $(DDH_s(x_s) x_\Delta)_{lm}$ either has finite part only, which can be evaluated explicitly by replacing x_s by intervals $\mathcal{I}_{\hat{x}_s}$, or is of convolution type and has bandwidth at most $K(|D| - 1)$ (for $l, m = M + 1, \dots, M + N$). Since the factor $(A_\Delta)_{nl}$ has a non-vanishing finite part only, whenever $n = 1, \dots, M$ or $m = 1, \dots, M$ the product $(A_\Delta DDH_s(x_s) x_\Delta)_{nm}$ has non-vanishing finite part only. Moreover, for $n, m = M + 1, \dots, M + N$ arguments similar to the ones in Remark 6.3, but now for Q_1 with vanishing tail, imply that $(A_\Delta DDH_s(x_s) x_\Delta)_{nm}$ is of the form described in Lemma 5.1 with $K_1 = K(2|D| - 1)$ and $K_2 = K(|D|)$ and $y^* = 0$.

Similar, but somewhat more involved, arguments apply to the fourth term, i.e. (70). The first difference is that the finite part of A_s is s -dependent, hence we replace it by the interval-valued operator \mathcal{A}_s , see Section 8.3. The second difference is that the tail of \mathcal{A}_s does not vanish but instead is given by $i\mathbf{K}^{-1}I_K$. Hence Remark 6.3 now implies that for $n, m = M + 1, \dots, M + N$ the product $(A_s DDDH_s(x_s) x_\Delta x_\Delta)_{nm}$ is of the form described in Lemma 5.1 with $K_1 = K(2|D| - 1)$ and $K_2 = K(|D|)$ and $y^* = \frac{1}{K+1}|y^{[n,m]}|$ for some $y^{[n,m]} \in \ell_\nu^1$ (depending on n and m) with at most $K(|D| - 1)$ non-vanishing modes, which can be computed explicitly using interval arithmetic, once again replacing x_s by $\mathcal{I}_{\hat{x}_s}$.

In summary, in view of the above arguments, it follows that

$$D_s D_s (A_s (A_s^\dagger - DH_s(x_s)))_{nm}$$

has a non-vanishing finite part only whenever $n = 1, \dots, M$ or $m = 1, \dots, M$, whereas it is of the form described in Lemma 5.1 with $K_1 = K(2|D| - 1)$ and $K_2 = K(|D|)$ and $y^* = \frac{1}{K+1}y^{[n,m]}$. We conclude that

$$\left\| \max_{s \in [0,1]} |D_s D_s ((A_s(A_s^\dagger - DH_s(x_s)))_{nm}) \right\|$$

can be bounded explicitly using a direct computation and applying Lemma 5.1. This concludes the Z_1 estimate.

8.4.3 The Z_2^s bound

We generalize the estimate from Section 6.3.3. We apply the mean value theorem and the triangle inequality to estimate

$$\begin{aligned} & \max_{s \in [0,1]} \sup_{b, c \in B_r(0)} \|(A_s [DH_s(x_s) - DH_s(x_s + b)] c)_n\| \leq \\ & r^2 \sum_{m=1}^{M+N} \left[\max_{s \in [0,1]} \|(A_s)_{nm}\| \right] \left[\max_{s \in [0,1]} \sup_{\bar{b}, \bar{c} \in B_1(0)} \sup_{z \in B_{r_*}(0)} \|(DDH_s(x_s + z)\bar{b}\bar{c})_m\| \right], \end{aligned}$$

for any $r \leq r_*$. To estimate $\|(A_s)_{nm}\|$ uniformly in $s \in [0, 1]$ we simply use the triangle inequality to obtain

$$\|(A_s)_{nm}\| \leq (1-s)\|(A_0)_{nm}\| + s\|(A_1)_{nm}\| = \max\{\|(A_0)_{nm}\|, \|(A_1)_{nm}\|\}.$$

The factor $\|(DDH_s(x_s + z)\bar{b}\bar{c})_m\|$ is estimated in the same way as in Section 6.3.3. Introducing the notation $\hat{x}_s = ((\hat{\lambda}_s)_{j=1}^M, (\hat{v}_s)_{i=1}^N)$ for $s = 0, 1$, the only changes are that the intervals $[\hat{\lambda}_j - r_*, \hat{\lambda}_j + r_*]$ get replaced by

$$\left[\min \left\{ (\hat{\lambda}_0)_j, (\hat{\lambda}_1)_j \right\} - r_*, \max \left\{ (\hat{\lambda}_0)_j, (\hat{\lambda}_1)_j \right\} + r_* \right],$$

while $\|\hat{v}_i\|_\nu + r_*$ gets replaced by $\max\{\|(\hat{v}_0)_i\|_\nu, \|(\hat{v}_1)_i\|_\nu\} + r_*$.

8.5 Injectivity of A_s

The assumptions in Theorem 3.1 imply that

$$Z_n(\hat{r}) < \hat{r} \quad \text{for } n = 1, \dots, M + N. \quad (71)$$

Here we prove that the construction for the bounds $Z_n(r)$ in Section 8.4, when combined with (71), imply that A_s is injective for $s \in [0, 1]$. Indeed, by construction the splitting (64) implies that

$$Z_{0n} < 1 \quad \text{for } n = 1, \dots, M + N, \quad (72)$$

is a necessary condition for (71) to hold. Furthermore, the bound (72) implies that

$$\sup_{s \in [0,1]} \|I - A_s A_s^\dagger\|_{B(X,X)} < 1,$$

with the norm (10) on X . This in itself only implies that A_s is surjective for all $s \in [0, 1]$. Next we use the block structure of A_s :

$$A_s x = \mathbf{E} \left(\hat{A}_s \Pi_K x \right) - \mathbf{i} \mathbf{K}^{-1} \Pi_K^\infty x, \quad (73)$$

where $\hat{A}_s \stackrel{\text{def}}{=} (1-s)\hat{A}_0 + s\hat{A}_1$ is a square matrix of size $M + (2K+1)N$. It now follows from surjectivity of A_s that \hat{A}_s is surjective for any $s \in [0, 1]$. Since \hat{A}_s is finite dimensional, its surjectivity implies its injectivity, which in turn implies that A_s is injective due to its block structure (73) and the fact that \mathbf{K}^{-1} is injective on $\Pi_K^\infty X$.

We conclude that negativity of the radii polynomials implies, for the bounds construction in Section 8.4, that A_s is injective for all $s \in [0, 1]$, so that fixed points of T_s correspond to zeros of H_s .

9 Computational aspects

In this section we highlight some algorithmic aspects of continuation. In particular, we discuss how we vary the step size and the number of modes.

Within the framework of a standard predictor-corrector algorithm we would like to choose near optimal step sizes, i.e., for a fixed number of modes K we would like to curb computational cost by taking large steps while still obtaining a rigorous validation. We use a heuristic that is similar to the one introduced in [32]. Namely, we predict the size of a next successful step based on an extrapolation of the estimates obtained in the previous step. Such a prediction is feasible since we can analyze how the different bounds depend on the (extrapolated) step size. To fix ideas, let σ denote the ratio between the hypothesized step size and the current step size δ . Then all bounds that essentially arise from the *first* term in the right hand side of the interpolation estimate (8.1) are independent in σ , whereas all bounds that essentially arise from the *second* term in the right hand side of (8.1) are *quadratic* in σ to leading order. The Z_2 bound is not based on interpolation estimates and is independent of σ to leading order. We may thus interpret the radii polynomials $p_n(r)$ as descending from an expression $\tilde{p}_n(r, \sigma)$ through $p_n(r) = \tilde{p}_n(r, 1)$, where \tilde{p} is of the form

$$\tilde{p}_n(r, \sigma) = \tilde{Y}_0 + (\tilde{Z}_0 + \tilde{Z}_1 - 1)r + \tilde{Z}_2 r^2 + \sigma^2 [\tilde{Y}_0^\Delta + (\tilde{Z}_0^\Delta + \tilde{Z}_1^\Delta)r]. \quad (74)$$

When we have a successful validated continuation step, i.e., $p_n(r) = \tilde{p}_n(r, 1) < 0$ for all $n = 1, \dots, M + N$, then we determine the (approximately) largest $\sigma > 1$ for which we still have $\tilde{p}_n(\hat{r}, \sigma) < 0$ for all $n = 1, \dots, M + N$, where $\hat{r} = \frac{r_{\min} + r_{\max}}{2}$. We then update the stepsize according to the rule

$$\delta_{\text{new}} = \min \left(\frac{0.95 + \sigma}{2} \delta_{\text{old}}, 1.2 \right).$$

This is somewhat on the safe side, as it stabilizes at $\sigma = 1.05$, i.e., it has a margin of roughly 5%, since we prefer to avoid failing steps. Furthermore, the

stepsize is never increased by more than 20% at any step, thus avoiding risky increases.

While following a curve of periodic solutions, it may happen that the number of modes initially chosen for the validation is no longer suitable. If that happens, we want to increase or decrease the number of modes suitably. We use the following heuristic, settled on after limited experimentation, for the number of modes we require. $K_\epsilon \leq K$ be the smallest positive integer such that $\sum_{i=1}^N \|(\hat{v}_i)_k\| < \epsilon$ for all $|k| \geq K_\epsilon$ (in the code we chose $\epsilon = 10^{-14}$). Roughly speaking, we aim for one quarter of the modes to be smaller than ϵ , i.e., $K \approx \frac{4}{3}K_\epsilon$. For small K this has to be adjusted slightly. In particular, we change the number of modes. To be precise, we set

$$K_\epsilon^{\text{ref}} = \begin{cases} K - 5 & \text{if } K < 20 \\ \frac{3}{4}K & \text{if } K \geq 20 \end{cases}$$

and we adapt the number of modes K whenever $|\frac{K_\epsilon - K_\epsilon^{\text{ref}}}{K_\epsilon^{\text{ref}}}| > \frac{1}{10}$. In such a situation, we update $K_{\text{new}} = K_{\text{old}} + \Delta K$, where

$$\Delta K = \begin{cases} K_\epsilon - K_\epsilon^{\text{ref}} & \text{if } \left| \frac{K_\epsilon - K_\epsilon^{\text{ref}}}{K_\epsilon^{\text{ref}}} \right| > \frac{1}{10} \\ 0 & \text{otherwise.} \end{cases} \quad (75)$$

In order for subsequent steps in the continuation to “glue” together, see Remark 3.5, we go about changing the number of modes in the continuation algorithm as follows. At the end of a continuation step, we turn the endpoint of the previous step into the starting point \hat{x}_0 of the next step. For this point we compute ΔK .

If $\Delta K > 0$ then we increase K to $K_{\text{new}} > K_{\text{old}}$ and we pad \hat{x}_0 with zeros, i.e., we replace \hat{x}_0 by $\Pi_{K_{\text{new}}}\mathbf{E}\hat{x}_0$. Analogously, we pad \hat{q}_0 and \hat{x}_0 , which are used in the phase condition and continuation equation.

If $\Delta K < 0$ then we do not decrease $K = K_{\text{old}}$ yet, and we do not change \hat{x}_0 , but we choose $\hat{x}_1 \in \Pi_{K_{\text{new}}}X$ with $K_{\text{new}} = K_{\text{old}} + \Delta K < K_{\text{old}}$, and similarly for \hat{q}_1 and \hat{x}_1 . Then at the *next* step of the continuation we replace K by K_{new} .

In both cases, the step where the end points have a non-matching number of nontrivial modes is somewhat suboptimal from the point of view of the estimates, hence we decrease the step size by 10% when the number of modes increases.

In addition to adapting the number of modes as described above, we also increase K by two modes whenever

$$1 - (\tilde{Z}_0 + \tilde{Z}_1) < \sqrt{\delta^2 + 4\tilde{Y}_0\tilde{Z}_2}, \quad (76)$$

where the threshold δ is set at $\delta_0 = 0.1$, and we never decrease the number of modes (even when suggested by (75)) if inequality (76) is violated for $\delta = \delta_1 = 0.2$. To evaluate (76) we consider the parts of the continuation bounds that are independent of the step size, see (74).

10 Examples: continuous branches of solutions

To demonstrate the efficacy of the rigorous continuation method we present several examples. We first perform continuation in the van der Pol system (52) for $10^{-4} \leq \mu \leq 4$, effectively turning the pointwise diagram in Figure 4 into a proven smooth curve of solutions. In Figure 9 we depict the step size versus μ . The step size starts small for small μ and increases sharply at the beginning of the validation, but soon it plateaus and then decreases gradually until it suddenly drops sharply. This drop indicates a breakdown of the algorithm, which turns out to be due to Matlab providing a very inaccurate approximate inverse \hat{A} of $D\hat{H}(\hat{x})$. Indeed, the bound Z_0 becomes of order 1. On the one hand, this points to an inherent drawback of the radii polynomial approach, as obtaining a reasonably accurate numerical inverse of the Jacobian is a prerequisite. On the other hand, we could continue rigorous validation further along the branch by either tweaking the code to “trick” Matlab into providing a better inverse, or by forcing a better numerical inverse by computing the inverse using Intlab. The former is not very robust, while the latter is robust but has high computational cost. We note that single orbit validation at the same parameter value, see Figure 4, succeeds since the numerical approximate solution there has a different phase shift. Apparently, this leads to Jacobian (in which the coefficients are correspondingly rotated in the complex plane) for which Matlab *is* able to find a good numerical inverse. We did not investigate this implementation issue further.

The second example is a continuation in the Lorenz systems (55) with $\sigma = 10$, $\beta = 8/3$ and ρ varying. A branch of solutions is depicted in Figure 10. To illustrate the general applicability, we also couple 10 Lorenz systems ($N = 30$) in the following way

$$\begin{cases} \dot{x}_i = \sigma(y_i - x_i), \\ \dot{y}_i = x_i(\rho + i\epsilon - z_i) - y_{i-1}, \\ \dot{z}_i = x_i y_i - \beta z_i, \end{cases} \quad \text{for } i = 1, \dots, 10, \quad (77)$$

where in this case $\rho = 28$ and the new parameter ϵ is varying. Of course continuation is more time and memory consuming in this case. We depict a short continuation in Figure 11.

Our final example is the Rychkov system [24]

$$\begin{cases} \dot{u}_1 = u_2 - u_1^5 + u_1^3 - \mu u_1, \\ \dot{u}_2 = -u_1, \end{cases} \quad (78)$$

which is of order 5. In [16] the proof of the existence of a saddle node bifurcation was presented, for a parameter value μ^* in the interval $[0.224, 0.2249654]$. The code has no problem in following the periodic orbit through the fold. The norm of validated solution branch can be seen in Figure 12. A computer-assisted proof of the fact that exactly one saddle-node bifurcation occurs along this branch is one of the topics of the forthcoming paper [29].

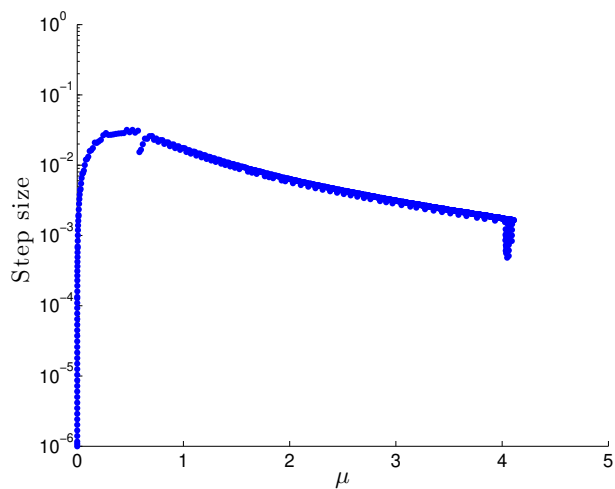


Figure 9: Step size versus μ . Some oscillation is noticeable in the step size. This is due to the fact that the stepsize is decreased when the number of modes is changed, see Section 9. During this validation, the number of modes has been increased automatically from 4 to about 400.

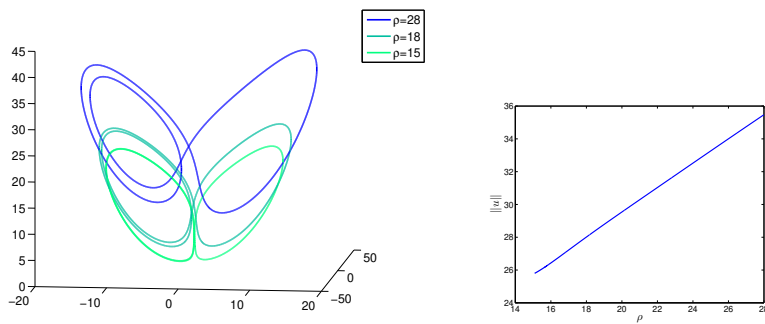


Figure 10: Validated continuation for the Lorenz system (55) from $\rho = 28$ to $\rho = 15.5$. In the left graph, the lower orbit still has two distinct swirls in the left lobe, but they are too close to each other to be seen in this graph.

References

- [1] Gianni Arioli and Hans Koch. Computer-assisted methods for the study of stationary solutions in dissipative systems, applied to the Kuramoto-Sivashinski equation. *Arch. Ration. Mech. Anal.*, 197(3):1033–1051, 2010.
- [2] Maxime Breden and Roberto Castelli. Existence and instability of steady states for a triangular cross-diffusion system: A computer-assisted proof. *Journal of Differential Equations*, 264(10):6418–6458, 2018.
- [3] Maxime Breden, Jean-Philippe Lessard, and Matthieu Vanicat. Global bifurcation diagrams of steady states of systems of pdes via rigorous numerics: a 3-component reaction-diffusion system. *Acta applicandae mathematicae*, 128(1):113–152, 2013.
- [4] CAPD: Computer assisted proofs in dynamics, a package for rigorous numerics. URL: <http://capd.i.i.uj.edu.pl/>.
- [5] Roberto Castelli. Rigorous computation of non-uniform patterns for the 2-dimensional gray-scott reaction-diffusion equation. *Acta Applicandae Mathematicae*, 151(1):27–52, 2017.
- [6] Alan R. Champneys and Björn Sandstede. Numerical computation of coherent structures. In *Numerical continuation methods for dynamical systems*, Underst. Complex Syst., pages 331–358. Springer, Dordrecht, 2007.
- [7] R.H. Clewley, W.E. Sherwood, M.D. LaMar, and J.M. Guckenheimer. PyDSTool, a software environment for dynamical systems modeling, 2007. URL: <https://sourceforge.net/projects/pydstool/>.
- [8] Anaïs Correc and Jean-Philippe Lessard. Coexistence of nontrivial solutions of the one-dimensional Ginzburg-Landau equation: a computer-assisted proof. *European J. Appl. Math.*, 26(1):33–60, 2015.
- [9] Harry Dankowicz and Frank Schilder. *Recipes for continuation*, volume 11 of *Computational Science & Engineering*. Society for Industrial and Applied Mathematics (SIAM), Philadelphia, PA, 2013. URL: <https://sourceforge.net/projects/cocotools/>.
- [10] S. Day, J.-P. Lessard, and K. Mischaikow. Validated continuation for equilibria of PDEs. *SIAM J. Numer. Anal.*, 45(4):1398–1424, 2007.
- [11] A. Dhooge, W. Govaerts, Yu. A. Kuznetsov, H. G. E. Meijer, and B. Sautois. New features of the software MatCont for bifurcation analysis of dynamical systems. *Math. Comput. Model. Dyn. Syst.*, 14(2):147–175, 2008. URL: <https://sourceforge.net/projects/matcont/>.
- [12] E.J. Doedel, B.E. Oldeman, A.R. Champneys, F. Dercole, T.F. Fairgrieve, Y. Kuznetsov, R.C. Paffenroth, B. Sandstede, X.J. Wang, and C.H. Zhang. AUTO-07p: Continuation and bifurcation software for ordinary differential equations, 2012. URL: <http://sourceforge.net/projects/auto-07p/>.

- [13] Bard Ermentrout. *Simulating, analyzing, and animating dynamical systems*, volume 14 of *Software, Environments, and Tools*. Society for Industrial and Applied Mathematics (SIAM), Philadelphia, PA, 2002. A guide to XPPAUT for researchers and students. URL: <http://www.math.pitt.edu/~bard/xpp/xpp.html>.
- [14] J.-Ll. Figueras, A. Haro, and A. Luque. Rigorous computer-assisted application of KAM theory: a modern approach. *Found. Comput. Math.*, 17(5):1123–1193, 2017.
- [15] Marcio Gameiro, Jean-Philippe Lessard, and Alessandro Pugliese. Computation of smooth manifolds via rigorous multi-parameter continuation in infinite dimensions. *Found. Comput. Math.*, 16(2):531–575, 2016.
- [16] Armengol Gasull, Héctor Giacomini, and Maite Grau. Effective construction of Poincaré-Bendixson regions. *J. Appl. Anal. Comput.*, 7(4):1549–1569, 2017.
- [17] Allan Hungria, Jean-Philippe Lessard, and Jason D Mireles James. Rigorous numerics for analytic solutions of differential equations: the radii polynomial approach. *Mathematics of Computation*, 85(299):1427–1459, 2016.
- [18] Yuri A. Kuznetsov. *Elements of applied bifurcation theory*, volume 112 of *Applied Mathematical Sciences*. Springer-Verlag, New York, third edition, 2004.
- [19] Jean-Philippe Lessard. Recent advances about the uniqueness of the slowly oscillating periodic solutions of Wright’s equation. *J. Differential Equations*, 248(5):992–1016, 2010.
- [20] Jean-Philippe Lessard and J. D. Mireles James. Computer assisted Fourier analysis in sequence spaces of varying regularity. *SIAM J. Math. Anal.*, 49(1):530–561, 2017.
- [21] Jean-Philippe Lessard, J. D. Mireles James, and Julian Ransford. Automatic differentiation for Fourier series and the radii polynomial approach. *Phys. D*, 334:174–186, 2016.
- [22] K. Makino and M. Berz. Rigorous integration of flows and odes using taylor models. In *Proceedings of the 2009 conference on Symbolic Numeric Computation*, pages 79–84, 2009.
- [23] Siegfried M Rump. Intlab—interval laboratory. In *Developments in reliable computing*, pages 77–104. Springer, 1999.
- [24] GS Rychkov. The maximum number of limit cycles of polynomial liénard systems of degree five is equal to two. *Differential Equations*, 11:301–302, 1975.

- [25] J. B. van den Berg, M. Breden, J.-P. Lessard, and M. Murray. Continuation of homoclinic orbits in the suspension bridge equation: a computer-assisted proof. *J. Differential Equations*, 264(5):3086–3130, 2018.
- [26] J. B. van den Berg, C. Groothedde, and J.-P. Lessard. A general method for computer-assisted proofs of periodic solutions in delay differential problems, 2018. Preprint.
- [27] J. B. van den Berg and J.-P. Lessard. Chaotic braided solutions via rigorous numerics: chaos in the Swift-Hohenberg equation. *SIAM J. Appl. Dyn. Syst.*, 7(3):988–1031, 2008.
- [28] J. B. van den Berg, J.-P. Lessard, and K. Mischaikow. Global smooth solution curves using rigorous branch following. *Math. Comp.*, 79(271):1565–1584, 2010.
- [29] J. B. van den Berg, J.-P. Lessard, and E. Queirolo. Rigorous verification of Hopf bifurcations in ODEs, 2018. In preparation.
- [30] J. B. van den Berg and E. Queirolo. MATLAB code for “A general framework for validated continuation of periodic orbits in systems of polynomial ODEs”, 2018. <https://www.math.vu.nl/~janbouwe/code/continuation/>.
- [31] J. B. van den Berg and R. Sheombarsing. Validated computations for connecting orbits in polynomial vector fields, 2018. In preparation.
- [32] J. B. van den Berg and J. F. Williams. Validation of the bifurcation diagram in the 2D Ohta-Kawasaki problem. *Nonlinearity*, 30(4):1584–1638, 2017.
- [33] Thomas Wanner. Computer-assisted bifurcation diagram validation and applications in materials science. In *Rigorous numerics in dynamics*, volume 74 of *Proc. Sympos. Appl. Math.*, pages 123–174. Amer. Math. Soc., Providence, RI, 2018.
- [34] Piotr Zgliczyński. Steady state bifurcations for the Kuramoto-Sivashinsky equation: a computer assisted proof. *J. Comput. Dyn.*, 2(1):95–142, 2015.